ESPOO 2008 VTT PUBLICATIONS 683

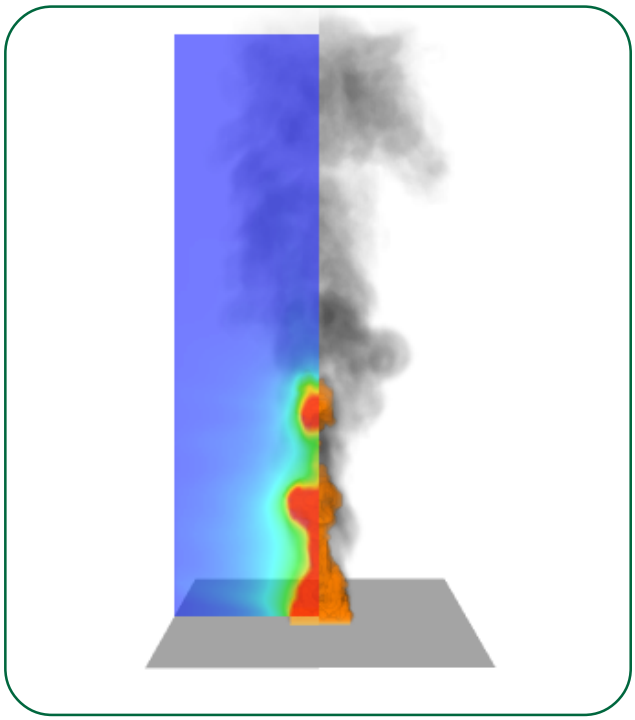

Simo Hostikka

# Development of fire simulation models for radiative heat transfer and probabilistic risk assessment

VTT PUBLICATIONS 683

# Development of fire simulation models for radiative heat transfer and probabilistic risk assessment

Simo Hostikka

*Thesis for the degree of Doctor of Technology to be presented with due permission for public examination and criticism in Lecture Room E at Helsinki University of Technology on the 6th of June, 2008, at 12 o'clock noon.*

ISBN 978-951-38-7099-7 (soft back ed.)
ISSN 1235-0621 (soft back ed.)

ISBN 978-951-38-7100-0 (URL: http://www.vtt.fi/publications/index.jsp)
ISSN 1455-0849 (URL: http://www.vtt.fi/publications/index.jsp)



JULKAISIJA – UTGIVARE – PUBLISHER

VTT, Vuorimiehentie 3, PL 1000, 02044 VTT
puh. vaihde 020 722 111, faksi 020 722 4374

VTT, Bergsmansvägen 3, PB 1000, 02044 VTT
tel. växel 020 722 111, fax 020 722 4374

VTT Technical Research Centre of Finland, Vuorimiehentie 3, P.O. Box 1000, FI-02044 VTT, Finland
phone internat. +358 20 722 111, fax + 358 20 722 4374

VTT, Kivimiehentie 4, PL 1000, 02044 VTT
puh. vaihde 020 722 111, faksi 020 722 4815

VTT, Stenkarlsvägen 4, PB 1000, 02044 VTT
tel. växel 020 722 111, fax 020 722 4815

VTT Technical Research Centre of Finland, Kivimiehentie 4, P.O. Box 1000, FI-02044 VTT, Finland
phone internat. +358 20 722 111, fax +358 20 722 4815

Edita Prima Oy, Helsinki 2008

Hostikka, Simo. Development of fire simulation models for radiative heat transfer and probabilistic risk assessment [Tulipalon simuloinnissa käytettävän säteilylämmönsiirtomallin ja riskianalyysimenetelmän kehittäminen]. Espoo 2008. VTT Publications 683. 103 p. + app. 82 p.

**Keywords** fire simulation, Monte Carlo simulation, probabilistic risk assessment, thermal radiation, verification, validation

# Abstract

An essential part of fire risk assessment is the analysis of fire hazards and fire propagation. In this work, models and tools for two different aspects of numerical fire simulation have been developed. The primary objectives have been firstly to investigate the possibility of exploiting state-of-the-art fire models within probabilistic fire risk assessments and secondly to develop a computationally efficient solver of thermal radiation for the Fire Dynamics Simulator (FDS) code.

In the first part of the work, an engineering tool for probabilistic fire risk assessment has been developed. The tool can be used to perform Monte Carlo simulations of fires and is called the Probabilistic Fire Simulator (PFS). In Monte Carlo simulation, the simulations are repeated multiple times, covering the whole range of variability of the input parameters and thus resulting in a distribution of results covering what can be expected in reality. In practical applications, advanced simulation techniques based on computational fluid dynamics (CFD) are needed because the simulations cover large and complicated geometries and must address the question of fire spreading. Due to the high computational cost associated with CFD-based fire simulation, specialized algorithms are needed to allow the use of CFD in Monte Carlo simulation. By the use of the Two-Model Monte Carlo (TMMC) technique, developed in this work, the computational cost can be reduced significantly by combining the results of two different models. In TMMC, the results of fast but approximate models are improved by using the results of more accurate, but computationally more demanding, models. The developed technique has been verified and validated by using different combinations of fire models, ranging from analytical formulas to CFD.

In the second part of the work, a numerical solver for thermal radiation has been developed for the Fire Dynamics Simulator code. The solver can be used to compute the transfer of thermal radiation in a mixture of combustion gases, soot particles and liquid droplets. The radiative properties of the gas-soot mixture are computed using a RadCal narrow-band model and spectrally averaged. The three-dimensional field of radiation intensity is solved using a finite volume method for radiation. By the use of an explicit marching scheme, efficient use of look-up tables and relaxation of the temporal accuracy, the computational cost of the radiation solution is reduced below 30% of the total CPU time in engineering applications. If necessary, the accuracy of the solution can be improved by dividing the infrared spectrum into discrete bands corresponding to the emission bands of water and carbon dioxide, and by increasing the number of angular divisions and the temporal frequency. A new model has been developed for the absorption and scattering by liquid droplets. The radiative properties of droplets are computed using a Mie-theory and averaged locally over the spectrum and presumed droplet size distribution. To simplify the scattering computations, the single-droplet phase function is approximated as a sum of forward and isotropic components. The radiation solver has been verified by comparing the results against analytical solutions and validated by comparisons against experimental data from pool fires and experiments of radiation attenuation by water sprays at two different length scales.

Hostikka, Simo. Development of fire simulation models for radiative heat transfer and probabilistic risk assessment [Tulipalon simuloinnissa käytettävän säteilylämmönsiirtomallin ja riskianalyysimenetelmän kehittäminen]. Espoo 2008. VTT Publications 683. 103 s. + liitt. 82. s.

**Keywords** fire simulation, Monte Carlo simulation, probabilistic risk assessment, thermal radiation, verification, validation

# Tiivistelmä

Paloriskien arvioinnissa on olennaista palon seurausten ja leviämismahdollisuuksien analysointi. Tässä työssä on kehitetty tulipalojen numeerisen simuloinnin malleja ja työkaluja. Työn päätavoitteita ovat olleet palosimuloinnin parhaimpien laskentamallien hyödyntäminen todennäköisyyspohjaisessa paloriskien arvioinnissa sekä laskennallisesti tehokkaan säteilylämmönsiirron ratkaisijan kehittäminen Fire Dynamics Simulator -ohjelmaan.

Työn ensimmäisessä osassa on kehitetty insinöörikäyttöön soveltuva, Probabilistic Fire Simulator (PFS) -niminen työkalu paloriskien arviointiin. PFS-työkalulla tulipaloa voidaan tutkia Monte Carlo -menetelmällä, jossa simulointeja toistetaan useita kertoja satunnaisilla syöteparametrien arvoilla, jolloin yksittäisen numeroarvon sijaan tuloksena saadaan tulosten jakauma. Käytännön sovelluksissa tarvitaan numeeriseen virtauslaskentaan perustuvia simulointimenetelmiä, koska simuloitavat tilavuudet ovat suuria ja monimutkaisia ja koska niissä pitää pystyä simuloimaan palon leviämistä. Monte Carlo -menetelmän toteutuksessa on tällöin käytettävä tehtävään sopivia erikoismenetelmiä, koska virtauslaskenta on laskennallisesti raskasta ja aikaa vievää. Tässä työssä kehitetyn Kahden mallin Monte Carlo -menetelmän avulla laskentaa voidaan nopeuttaa yhdistämällä kahden eritasoisen mallin tulokset. Nopeasti ratkaistavan mutta epätarkan mallin tuottamia tuloksia parannetaan hitaammin ratkaistavan mutta tarkemman mallin avulla. Menetelmää on testattu erilaisilla palomallien yhdistelmillä aina analyyttisistä kaavoista virtauslaskentaan asti.

Työn toisessa osassa on kehitetty säteilylämmönsiirron numeerinen ratkaisija Fire Dynamics Simulator -ohjelmaan. Ratkaisija laskee säteilyn etenemistä palokaasuja, nokea ja nestepisaroita sisältävässä väliaineessa. Palokaasujen ja noen muodostaman seoksen säteilyominaisuudet lasketaan keskiarvoistamalla RadCal-kapeakaistamallin tulokset aallonpituuden yli. Lämpösäteilyn eteneminen ratkaistaan säteilylämmönsiirron kontrollitilavuusmenetelmällä. Säteilyratkaisijan vaatima laskenta-aika saadaan alle 30 %:iin kokonaislaskenta-ajasta käyttämällä eksplisiittistä ratkaisumenetelmää ja tehokkaita taulukkohakuja sekä luopumalla ratkaisun aikatarkkuudesta. Tarkkuutta voidaan tarvittaessa parantaa jakamalla tarkasteltava aallonpituusalue veden ja hiilidioksidin tärkeimpiä absorptiokaistoja vastaaviin osiin sekä tihentämällä diskretointia avaruuskulman ja ajan suhteen. Työssä on kehitetty uusi laskentamalli nestepisaroiden ja säteilyn vuorovaikutukselle. Pisaroiden säteilyominaisuudet lasketaan Mie-teorian avulla ja keskiarvoistetaan sekä spektrin että pisarakokojakauman yli. Yksittäisen nestepisaran sirottaman energian vaihefunktiota approksimoidaan eteenpäin siroavien ja isotrooppisten komponenttien summana. Säteilyratkaisijaa on testattu vertaamalla laskettuja tuloksia analyyttisiin ja kokeellisiin tuloksiin.

# Preface

This work has been carried out during 1997–2007 under the auspices of the VTT Technical Research Centre of Finland, and the Building and Fire Research Laboratory of National Institute of Standards and Technology (NIST), USA, where I worked as a guest researcher.

I am grateful to my supervisor, Dr. Olavi Keski-Rahkonen, who originally introduced me to the scientific approach to fire and fire technology. At the age of 12, I had joined Vehkalahti volunteer fire brigade, to which I wish to express my gratitude, but during my studies at Helsinki University of Technology, I already thought that fire, as interesting as it had been, was in my past. With his enthusiasm to for fire dynamics, Dr. Keski-Rahkonen showed that fire might become my profession and the source of challenges for research. Dr. Keski-Rahkonen is my co-author in two of the papers of this thesis.

The favourable and encouraging attitude of Prof. Rolf Stenberg from the Institute of Mathematics at Helsinki University of Technology is greatly acknowledged. I thank Prof. Frederick W. Mowrer and Dr. Stewart Miles for reading the manuscript and suggesting numerous improvements.

I have had the privilege to have a group of wonderful colleagues at two research organizations, VTT and NIST. To these people and especially to the co-authors of the papers, I wish to express my gratitude. The most important of my colleagues and co-authors has been Dr. Kevin McGrattan of NIST. His commitment and self-sacrifice have been essential for our successful co-operation. From the very first moment when I visited NIST and later when my wife, Salla, and I lived in Maryland, I have constantly been overtaken by the hospitality and friendship of the entire McGrattan family.

I wish to thank my wife Salla – the most important person in my life – for the love and encouragement, and our children Helka, Kerkko, Iisak and Atro for sharing my attention during the preparation of this thesis. I also wish to thank my parents Raita and Veikko Hostikka for their endless support and trust.

Finally, I thank my Heavenly Father for everything He has done, and all the victories I have already won.

# List of publications

The dissertation is based on the following publications, which are referred to in the text by Roman numerals I–V:

I Hostikka, S. & Keski-Rahkonen, O. Probabilistic simulation of fire scenarios. Nuclear engineering and design, 2003. Vol. 224, No. 3, pp. 301–311.

II Hostikka, S., Korhonen, T. & Keski-Rahkonen, O. Two-model Monte Carlo simulation of fire scenarios. In: Gottuk, D. & Lattimer, B. (Eds.). Proceedings of the Eighth International Symposium on Fire Safety Science. Beijing, China, 18–23 Sept. 2005. International Association for Fire Safety Science, 2005. Pp. 1241–1252.

III Floyd, J.E., McGrattan, K.B., Hostikka, S. & Baum, H.R. CFD fire simulation using mixture fraction combustion and finite volume radiative heat transfer. Journal of Fire Protection Engineering, 2003. Vol. 13, No. 1, pp. 11–36.

IV Hostikka, S., McGrattan, K.B. & Hamins, A. Numerical modeling of pool fires using LES and finite volume method for radiation. In: Evans, D.D. (Ed.). Proceedings of the Seventh International Symposium on Fire Safety Science. Worcester, MA, 16–21 June 2003. International Association for Fire Safety Science, 2003. Pp. 383–394.

V Hostikka, S. & McGrattan, K. Numerical modeling of radiative heat transfer in water sprays. Fire Safety Journal, 2006. Vol. 41, No. 1, pp. 76–86.

# Author's contribution

Paper I deals with the development of a probabilistic approach and tool for fire simulations. The author implemented the first version of Probabilistic Fire Simulator software, performed the application simulations and did most of the writing. Paper II is an extension of the probabilistic tool to more complicated scenarios. The software was implemented jointly with the co-author, Dr. Timo Korhonen but the model formulation, actual application simulations and most of the writing were made by the author. In papers I–II, the formulation of the general approach and analysis of the results were made jointly by Dr. Olavi Keski-Rahkonen, who supervised the work.

Papers III–V deal with the development of Fire Dynamics Simulator (FDS) computer code. Paper III is a general description of the major development steps that were taken during 2000–2001 when the author worked as a guest researcher at NIST, developing and implementing a new computational model for thermal radiation. In Paper III, the author contributed to the description of Finite Volume Radiation Model. In Paper IV, the author is responsible for the computations, analysis of the results and most of the writing.

Paper V deals with the extension of the radiation model described in Papers III–IV to account for the interaction of thermal radiation and liquid droplets. Water sprays were used as an application. The author is solely responsible for the model development, computations and writing the paper. All the model implementations to FDS code were made in close co-operation with Dr. Kevin McGrattan of NIST.

# Contents

# List of symbols and abbreviations

| | |
|---|---|
| $A$ | cell face area |
| $B$ | radiative emission term |
| $C$ | cross sectional area (absorption or scattering) |
| $c$ | speed of light |
| $d$ | droplet diameter |
| $e_{\lambda b}$ | Planck's spectral distribution of emissive power |
| $E_3$ | exponential integral function (order 3) |
| $f$ | probability density function |
| $F$ | probability distribution function |
| $g$ | limit state function |
| $I$ | intensity |
| $ijk$ | cell indices |
| $P$ | probability |
| $\dot{\mathbf{q}}''$ | heat flux vector |
| $m$ | cell index |
| $N$ | number of random samples, spectral bands or solid angles, droplet number density |
| $\mathbf{n}$ | cell face normal vector |
| $n$ | number of random variables, spectral band |
| $r$ | droplet radius |
| $\mathbf{s}$ | unit direction vector |
| $T$ | temperature |
| $t$ | time |
| $t_g$ | growth time of the heat release rate |
| $U$ | total combined intensity |
| $V_{ijk}$ | cell volume |
| $\mathbf{x}$ | random vector, position vector |
| $\mathbf{x}_s$ | scaling point |
| $x$ | random variable |

**Greek**

| | |
|---|---|
| $\chi_f$ | forward scattering fraction |
| $\chi_r$ | local radiative fraction |
| $\partial\Omega^l$ | discretized solid angle |
| $\varepsilon$ | surface mean hemispherical emissivity |
| $\Phi$ | scaling function, scattering phase function |
| $\phi$ | joint density function, azimuthal angle |

| | |
|---|---|
| $\kappa$ | absorption coefficient |
| $\lambda$ | wavelength |
| $\Omega$ | random space, solid angle |
| $\theta$ | polar angle |
| $\rho$ | density |
| $\sigma$ | scattering coefficient, Stefan-Boltzmann constant |

**Subscripts**

| | |
|---|---|
| *d* | droplet |
| *m* | mean droplet property |
| $\lambda$ | spectral value |
| *n* | average over spectral band |
| *r* | radiant |
| *x,y,z* | co-ordinate directions |
| *w* | water |

**Abbreviations**

| | |
|---|---|
| CFD | Computational Fluid Dynamics |
| CFL | Courant-Friedrichs-Lewy |
| DNS | Direct Numerical Simulation |
| FDS | Fire Dynamics Simulator |
| EBU | Eddy Break-Up |
| DOM | Discrete Ordinates Methods |
| DT | Discrete Transfer |
| FVM | Finite Volume Method |
| LES | Large Eddy Simulation |
| LHS | Latin Hypercube Sampling |
| MC | Monte Carlo |
| NPP | Nuclear Power Plant |
| PFS | Probabilistic Fire Simulator |
| PRA | Probabilistic Risk Assessment |
| PSA | Probabilistic Safety Assessment |
| RANS | Reynolds-Averaged Navier-Stokes |
| RTE | Radiation Transport Equation |
| SRS | Simple Random Sampling |
| TMMC | Two-Model Monte Carlo |

# Part I
# Probabilistic simulation of fires

# 1. Introduction

The primary purpose of fire safety engineering is to ensure that the risk of fire induced losses for humans, property, environment and the surrounding society associated with the target of the analysis is acceptable by the common standards of the society. Additional objectives may be imposed, for example by economical goals and needs to protect cultural heritage. Fire safety engineering is typically used to design the fire safety measures of new buildings or transportation vehicles. Traditionally, the design is based on a set of requirements for the physical characteristics, such as the dimensions of the fire compartments, classification of structures and width and length of evacuation routes. These requirements are described in the national building codes and are based mainly on experimental findings and lessons learned from past fires. An alternative way, currently applicable in most countries in some form, is the use of the performance-based design, or alternative design as it is called in the ship industry. In a performance-based design method, the effectiveness of the fire safety measures is studied considering the performance of an entire system, not as fulfilment of individual requirements given by the building code. As a result, the apparent safety level of individual components of the system may be higher or lower, but the total risk level should be at least as good as using the traditional way. Definition of the acceptable risk level is still very much an open question in the context of building design. However, an essential part of the design process is the analysis of the risks associated with fires and the assessment of the efficiency of proposed fire safety measures.

The roots of modern risk analysis are in the 19$^{th}$ century, when both probability theory and scientific methods to assess the health effects of hazardous activities were developed [1]. For example, the probability of dying was calculated for insurance purposes. Conceptual development of risk analysis in industrially developed countries started from two directions: (1) with the development of nuclear power plants and concerns about their safety, and (2) with the establishment of governmental institutions for the protection of the environment, health and safety as a response to a rapid environmental degradation [1]. The development of *fire* risk analysis has been considerably slower than on the other fields because fire as a physical phenomenon is extremely difficult to model on a real scale. The complexity of fire modelling results from the multitude of

physical problems and chemical reactions to be solved simultaneously and the wide range of associated time and length scales. A lack of resources for fire research and education may also be a partial explanation for the relatively slow development. Sufficiently accurate computational models for fires have been introduced during the last two or three decades, and the development of computational resources has allowed their use in probabilistic fire risk analysis during just the last few years. The computational models are discussed in detail in the second part of the thesis.

An important field of fire risk analysis is the probabilistic risk assessment (PRA) of nuclear power plants (NPP). The first systematic application of PRA[1] to study the probabilities and consequences of severe reactor accidents in commercial NPPs was made in WASH-1400 [2] ("Rassmussen report"). WASH-1400 was later updated in NUREG-1150 [3]. In PRA, the fire risk analysis is performed in pieces, typically for one room or class of rooms at the time. Individual damage probabilities are not used directly to make judgements on the plant safety, but weighted by the ignition frequencies and used as node probabilities in the event or fault trees, thus contributing to the probability of severe accidents and overall assessment of the safety [4]. Most early attempts of fire PRA were qualitative, since the fire consequences were usually assumed, rather than predicted using some physically realistic models. A PRA guide [5] introduced three methods for fire propagation analysis, with zone model simulations being the most advanced one, and was based on the use of a few selected scenarios, which was a big step compared to the first generation conservative assumptions. A four-phase procedure proposed in [5] is still valid: (Task 1) fire hazard analysis to identify the critical plant areas and fire frequencies, (Task 2) fire propagation analysis, (Task 3) plant and system analysis to estimate the likelihood of fires leading to damage states, and (Task 4) release frequency analysis. However, the procedure still lacked the possibility to be truly quantitative because the choice of fire scenarios was based on expert opinion. In this work, computational tools are developed for the assessment of conditional fire damage probabilities in a way that has a potential to become truly quantitative by covering the distributions of input parameters and using sufficiently detailed fire models. Expert opinions are still needed in the selection of the rooms and targets to be modelled. The

[1] An alternative term is Probabilistic Safety Assessment (PSA).

development work has been part of the Finnish nuclear power plant safety research programmes [6, 7] with a central goal of improving the deterministic and stochastic tools for fire-PRA. During the work, both small additions and total re-interpretations have been made for Tasks 1–3 of the four phase procedure mentioned above [8, 9].

In the analysis of large and complicated targets, both the existing ones and the ones to be designed, the various techniques of fire risk analysis are usually combined. Qualitative and semi-quantitative methods, such as the fire risk index [10], are fast and simple to use and may be sufficient in some cases. Quantitative techniques such as event and fault trees can be used to manage the complex chains of safety measures, and are the fundamental parts of probabilistic fire risk analysis. One problem of using event trees is the static nature of the tree. Early attempts to bring in the time component to event tree analysis were made in the context of fire spreading [11, 12] and recently in the context of structural safety [13]. Expert judgement is always needed to focus the analysis to the most relevant regions and Bayesian techniques can be used to reduce the uncertainty in the probability estimates by utilizing the observed evidence [14]. The risk analysis techniques may be used to compute probabilities of individual pre-defined events or a general relation between the probability and the hazard severity, in which case the results can be conveniently presented as FN-curves [15, 16, 17]. In FN-curves, the probability of an event is plotted against the severity measure of the event, such as number of fatalities. The role of the fire statistics as a source of information for risk analysis has been studied at VTT by Tillander and Keski-Rahkonen [18,19]. The importance of the fire statistics was recently discussed by Sekizawa [20].

The practical technique for the combination of deterministic fire models to the probabilistic treatment of model variables has been the use of Monte Carlo simulation (MC). In MC, the uncertainty or statistical nature of the initial and boundary conditions can be taken into account rigorously by sampling the model variables randomly from their given distributions and computing a large number of model realizations leading to a distribution of all the potential outcomes that could occur under these uncertainties [21]. The term “Monte Carlo” refers to the application of probabilistic thinking in the computation of the probability of a successful outcome of a game of solitaire [22]. A guide for using MC in the quantitative risk analysis has been written by Vose [23]. Examples of the use of

MC simulations in the PSA work are found in the articles of Hofer and his co-authors [24, 25]. In Paper I of this thesis, a similar approach was chosen to compute the component failure probabilities in NPP cable tunnels and electronics rooms. Within the NPP fire safety projects at VTT, the computational tools were implemented in Probabilistic Fire Simulator (PFS) software [26]. For efficiency reasons, MC is often performed using Latin Hypercube Sampling [27, 28] rather than simple random sampling.

In fire safety engineering, MC simulations can be used for at least two purposes: integration over the statistical distributions to deduce the probability, and for propagation of uncertainty [29]. However, Hofer et al. [30, 31] have shown that the separation of these two purposes is not necessary since both sources of randomness can be taken into account within the same single-stage MC. The fast increase of computational resources during the last 10 years has made it possible to use numerical fire models within the MC simulation. In the context of fire safety engineering, Monte Carlo simulations have been used for instance to model the risks to human life due to PCB-contaminated oil fires [32] and building fires [33], to model fires at dwellings [34], assembly halls [35] and office buildings [36] and the probability of fire deaths due to toxic gas inhalations [37]. Computer tools such as CRISP [38, 34, 36] and CESARE-RISK [37, 39] that include the possibility for MC simulations were developed in the 1990s. Notarianni used Monte Carlo simulation and a two-zone fire model to study the role of uncertainty in fire regulations [40]. Some recent applications of Monte Carlo simulations include the following: the computation of the probability of reaching critical temperatures in steel members [41], the introduction of a probabilistic aspect to fire resistance specification for regulatory purposes [42], the identification of the most critical factors in determining the cost-benefit ratio for sprinkler installation in parking buildings [43], as well as the computation of the failure probabilities of fire detection system designs [44] and structural reliability [39]. In the studies mentioned above, fires were typically modelled using simple hand calculation formulas of zone models because the use of more advanced models has been computationally too expensive. In Paper II of this thesis, the Monte Carlo technique has been extended to allow the use of state-of-the art fire models like CFD as a computational tool. Additional examples of the use of the new technique can be found in reference [9].

# 2. Development of Probabilistic Fire Simulator

## 2.1 Monte Carlo simulation of fires

Monte Carlo (MC) simulation is a method of performing "numerical experiments" using random numbers and computers. An introduction to the mathematical aspects of MC simulations can be found in [45]. Several textbook level references can be found on the use of MC simulation in physics, for example see [46], and in risk analysis [21, 23]. Only a short description of the technique is given here, with an emphasis on the specific application to fire safety.

The question set by the PRA process is usually the following: "What is the probability of event $A$ in case of fire?" Examples of target events are the failure of a certain component or system, activation of a heat detector, smoke filling, flashover, extinction of the fire and fire death. The probability of event $A$ is a function of all possible factors that may affect the development of the fire and the systems' reaction to it. The affecting variables, denoted by a vector $\mathbf{X} = (X_1 \; X_2 \; \ldots \; X_n)^T$, are considered random variables, since the exact values of these variables are not known. Instead, they are associated with probability distributions with density functions by $f_i$ and distribution functions by $F_i$. The occurrence of the target event $A$ is indicated by a limit state function $g(t,\mathbf{x})$, which depends on time $t$ and vector $\mathbf{x}$ containing the values of the random variables. As an example of the target event, we consider the loss of some component. The limit state condition is now defined using function $g(t,\mathbf{x})$:

$$\begin{aligned} g(t,\mathbf{x}) &\le 0, \text{ if the component is lost at time } t \\ g(t,\mathbf{x}) &> 0, \text{ if the component is not lost at time } t \end{aligned} \tag{1}$$

The development of fire and the response of the components under consideration are assumed to be fully deterministic processes where the same initial and boundary conditions always lead to the same final state. With this assumption, the probability of event $A$ can now be calculated by the integral

$$P_A(t) = \iint\cdots\int_{\{\mathbf{x}|g(t,\mathbf{x})\le 0\}} \phi_x(\mathbf{x})dx_i \qquad (2)$$

where $\phi_X$ is the joint density function of variables **X**. The assumption of deterministic processes is valid if the epistemic uncertainty of the applied deterministic models is small as compared with the uncertainties caused by the input distributions. In practice, this means that all the relevant processes can be explicitly depicted as mathematical models that are numerically stable and sufficiently accurate. In highly non-linear problems, such as fire spread, these requirements may sometimes be difficult to meet.

In this work, the probability $P_A$ is calculated using Monte Carlo simulations where input variables are sampled randomly from the distributions $F_i$. The usability of the Monte Carlo simulation often depends on the number of random samples $N$ required for a sufficient degree of accuracy. If $N$ is large and $g(t,\mathbf{x})$ is expensive to evaluate, the computational cost of the MC simulation may become very high. For large $N$, the error of the simple random sampling (SRS) decreases as $1/\sqrt{N}$ according to the central limit theorem [47]. The convergence rate of the simulation can be improved by using sampling schemes that have smaller variance than SRS. Examples of more advanced sampling schemes are the use of quasi-random numbers, importance sampling and stratified sampling [45].

The simulations are made using a stratified sampling scheme called Latin Hypercube Sampling (LHS) [27]. In stratified sampling, the random space is divided into a discrete number of intervals in the direction of each random variable. As the number of samples from each interval is the same, the samples are given weights based on the total probability of the intervals. The advantage of the stratification is that the random samples are generated from all the ranges of possible values, thus giving insight into the tails of the probability distributions. In LHS, the $n$-dimensional parameter space is divided into $N^n$ cells. Each random variable is sampled in a fully stratified way and then these samples are attached randomly to produce $N$ samples from $n$ dimensional space. LHS will decrease the variance of the integral in equation (2) relative to the simple random sampling whenever the sample size $N$ is larger than the number of variables $n$ [48]. However, the amount of reduction increases with the degree of additivity in the random quantities on which the function being simulated depends. In fire simulations, the simulation result may often be a strongly

nonlinear function of the input variables. For this reason, we cannot expect that LHS would drastically decrease the variances of the probability integrals. Problems related to LHS with small sample sizes are discussed by Hofer [49] as well as by Pebesma & Heuvelink [50].

## 2.2 Two-Model Monte Carlo simulations

The numerical simulation of the complicated physical processes is always trading between the desired accuracy of the results and the computational time required. Quite often, the same problem can be tackled by many different models with different physical and numerical simplifications. A good example of this is the fire simulation in which zone models provide a fast way to simulate the essential processes of the fire, being inevitably coarse in the physical resolution. As an alternative, computational fluid dynamics (CFD) models have potentially higher physical resolution and can describe more complicated physical phenomena. The time needed for the CFD computation may be several orders of magnitude longer than the time needed for the zone models. A technique is therefore needed which can combine the results of the different models in a computationally efficient way. In this work, we have developed a technique that allows the use of two different models in one Monte Carlo simulation, and is therefore called Two-Model Monte Carlo (TMMC). TMMC is based on the assumption that the ratio of the results given by two models has smooth variations when moving from point to point of the random space. Therefore, if one of the models is presumably more accurate than the other, the ratio calculated at some point of the random space can be used to scale the result of the less accurate model within the neighbourhood of the point. By using a relatively small number of scaling points, the scaling function or surface can be created. The technique can be compared to the use of response surfaces to model the Monte Carlo data [39]. Instead of using the data from the scaling points directly, they are used to improve the accuracy of the actual Monte Carlo. The TMMC model was originally presented in Paper II of the thesis.

We assume that we have two numerical models, A and B, which can calculate the physical quantity $a(\mathbf{x},t)$ depending on a parameter $\mathbf{x}$ and the time $t$. In our analysis, $\mathbf{x}$ is considered to be a random variable from a random space $\Omega$. Model B is more accurate than model A, but the execution time of model B is (much)

longer than model A. The models are used to get two estimates of the time series: $\widetilde{a}^{A}(\mathbf{x}_s,t)$ and $\widetilde{a}^{B}(\mathbf{x}_s,t)$. In TMMC, we assume that at any point **x** of the random space, the accuracy of the model A results can be improved by multiplying them with a scaling function, which is the ratio of model B time series to model A time series at some point $\mathbf{x}_s$ in the vicinity of the current point **x**. The points $\mathbf{x}_s$ are called scaling points.

In the beginning of the simulation, the random space is divided into distinct regions. A scaling function is then calculated for each region

$$\Phi(\mathbf{x}_s,t)=\frac{\widetilde{a}^{A}(\mathbf{x}_s,t)}{\widetilde{a}^{B}(\mathbf{x}_s,t)} \tag{3}$$

where $\mathbf{x}_s$ is the mid-point of the scaling region $\Omega_s$. This process is illustrated in the upper part of Figure 1 showing the two time series corresponding to models A and B, and the scaling function $\Phi(\mathbf{x}_s,t)$. During the Monte Carlo, the result of the model A is multiplied by the scaling function corresponding to the closest scaling point, to get the corrected times series $\widetilde{a}^{AB}(\mathbf{x},t)$

$$\widetilde{a}^{AB}(\mathbf{x}_s,t)=\Phi(\mathbf{x}_s,t)\cdot\widetilde{a}^{A}(\mathbf{x}_s,t),\quad \mathbf{x}\in\Omega_s \tag{4}$$

The correction is illustrated in the lower part of Figure 1 showing again the time series A and B, and the corrected time series AB, which would be the result used within the TMMC. TMMC can provide significant time savings with respect to a full MC using model B because model B is used only in scaling points. The actual MC is still performed using model A. The magnitude of the time saving depends on the number of scaling points to the number of random points ratio.

Quite often, the result of the MC simulation is not the time series itself, but some scalar property derived from the time series. A typical result is the time to reach some critical value. A simplified version of the TMMC technique can be obtained if the scaling is done for scalar numbers directly. Although the scaling would be easier to implement for the scalars than for the whole time series, the simplification has some unwanted properties, which are demonstrated in Paper II of the thesis.

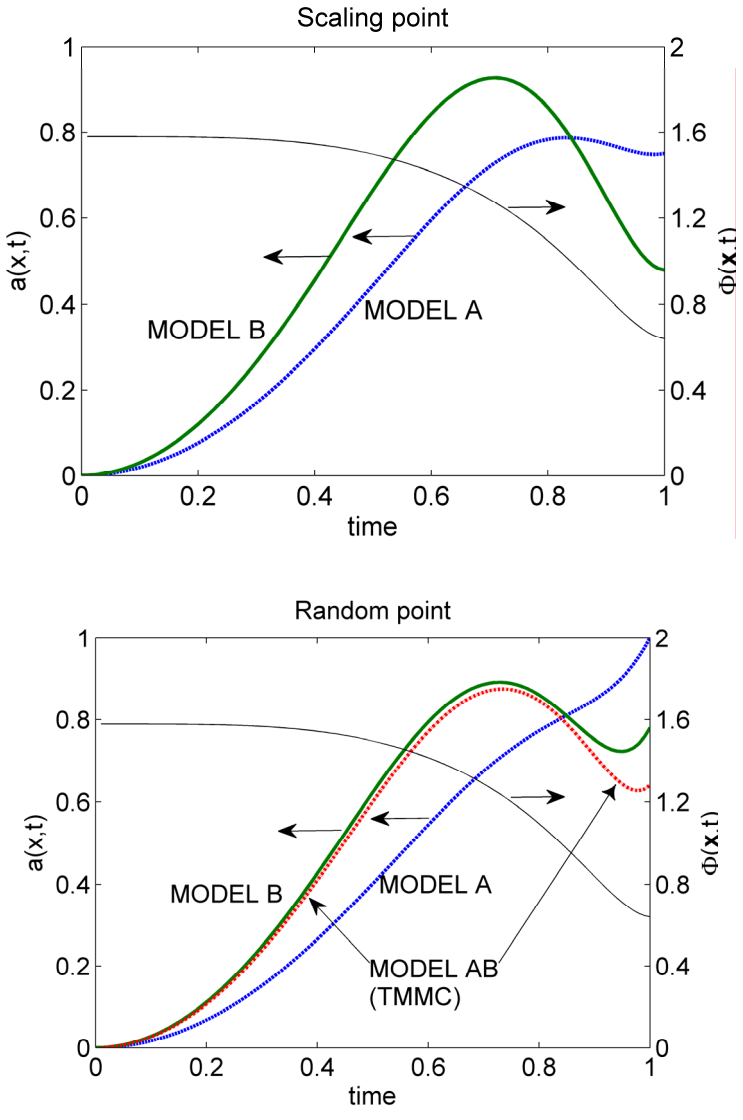


*Figure 1. An example of TMMC scaling. Time series* $\tilde{a}^{A}(\mathbf{x},t)$ *and* $\tilde{a}^{B}(\mathbf{x},t)$ *and scaling function* $\Phi(\mathbf{x}_s,t)$ *at scaling point (upper figure) and random point (lower figure). The lower figure also shows the estimate* $\tilde{a}^{AB}(\mathbf{x},t)$.

For a general function $a(x,t)$, it is not possible to tell how fast the function $\tilde{a}^{AB}(\mathbf{x},t)$ converges towards $\tilde{a}^{B}(\mathbf{x},t)$, when the number of scaling points is increased. However, it is clear that

$$\lim_{N_s \to \infty} \tilde{a}^{AB}(\mathbf{x}_s, t) = \tilde{a}^{B}(\mathbf{x}_s, t) \tag{5}$$

where $N_s$ is the number of scaling points.

## 2.3 Probabilistic Fire Simulator

The techniques described above have been implemented in a Probabilistic Fire Simulator tool (PFS). PFS has been developed at VTT in the projects concerning the fire safety of nuclear power plants [26], but applications are already much wider, covering the performance-based design of large buildings and ships. In addition to the actual Monte Carlo simulations, PFS can be used as an interface for several fire models: Fire Dynamics Simulator, CFAST [51], Ozone [52,53] and OptiMist [54].

PFS tool is implemented as a Microsoft Excel workbook including internal (Visual Basic) and external (Fortran DLL) subroutines for statistics and interfacing with the fire models. The first version of PFS [26] used commercial @Risk package for performing the Monte Carlo simulation and statistical operations, but in later versions, the necessary FORTRAN subroutines have been written for PFS.

# 3. Results and discussion

## 3.1 Scope

The results presented in this section fall into two categories: verification and validation. Verification is performed to ensure that the software has been implemented as planned and works as could be expected based on the provided documentation. Validation in turn deals with the actual accuracy of the software in the intended application. The verification problem is simple and fictitious but the validation problems are designed to be relevant for the software user. Some results from real applications can be found in [9].

## 3.2 Verification of TMMC

To verify the TMMC's capability to capture the cumulative distributions of scalar quantities, the technique is applied to the approximation of analytical function

$$a(x,t) = \min\left[e^{xt} - 1, 0.8 \cdot \left(e^{x} - 1\right)\right], \quad t \in [0,1] \tag{6}$$

The min-function is used to simulate a plateau of the time series reaching a steady state. In model A, the analytical function is approximated by a two term Taylor series expansion. Model B output is the function itself $\tilde{a}^{B}(x,t) = a(x,t)$. The random variable $x$ is distributed uniformly between 1 and 2. The actual outcome of the simulation, denoted by $c(x)$, is the time when $a(x,t)$ reaches a value $a_m = 2$ for the first time. Figure 2 shows the cumulative distributions of $c(x)$. The curve AB, corresponding to TMMC, is very close to the distribution of values derived from the exact function. As shown in Paper II, the scalar scaling would not produce good results in this particular case.

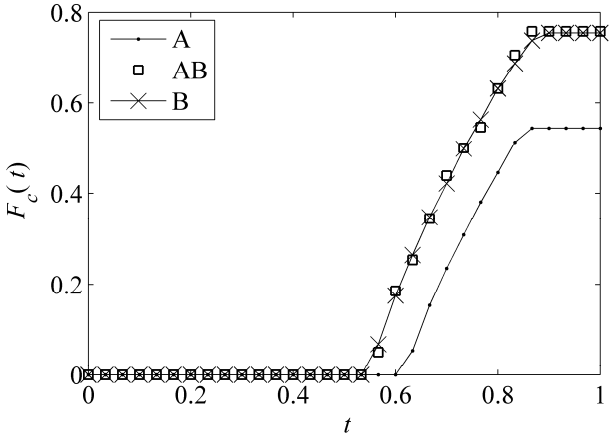


*Figure 2. Cumulative distributions of scalar quantities in the verification example. Curve B corresponds to the exact solution, curve A to its Taylor series approximation and curve AB to the TMMC estimate of the exact solution.*

## 3.3 Validation of TMMC

The possibilities to validate the probabilistic techniques are much more limited than the possibilities to validate the deterministic models, for which experimental data with well-defined boundary conditions can be found. Since the experimental data from a series of hundreds of fire tests is not available, the performance of the probabilistic fire simulation techniques is studied by performing numerical experiments. In the two validation tests, presented originally in Paper II, the reference result is obtained by performing a full MC analysis using the same model that is used as a basis for the scaling functions, i.e. Model B.

In the first validation test, Alpert's ceiling jet model [55] (Model A) and CFAST two-zone model (Model B) were used to predict the ceiling jet temperature under the ceiling of a 10 m × 10 m × 5 m (height) room with a fire in the middle of the floor. The room had one, 2.0 m × 2.0 m door to ambient. We simply assumed that in the current application, CFAST is more accurate than Alpert's model, whether this is true or not in reality. The validity of the applied tools is not relevant for the purpose of TMMC validation because we only want to validate the capability of TMMC to generate a useful correction for one model's

output using the output from another model. The actual model uncertainties become relevant in applications and should be evaluated in relation to the input uncertainties, as discussed in Section 2.1.

The fire heat release rate was of $t^2$-type with a random, uniformly distributed growth time $t_g$. Two scalar results were studied. The scalar result $b(t_g)$ was the ceiling jet temperature at time = 30 s. The scalar result $c(t_g)$ was the time to reach a critical temperature of 100 °C in the ceiling jet. The random space was divided into three sub domains. 1000 samples were calculated using both models. The predicted cumulative distributions of $b(t_g)$ are shown in the left part of Figure 3. At all values of $t_g$, CFAST predicted higher temperatures than Alpert's model. TMMC distribution was very close to the CFAST result, but had small discontinuities at the boundaries of the divisions. The right hand side of Figure 3 shows the cumulative distributions of $c(t_g)$. As can be seen, TMMC scaling very accurately captured the shape of the CFAST distribution.

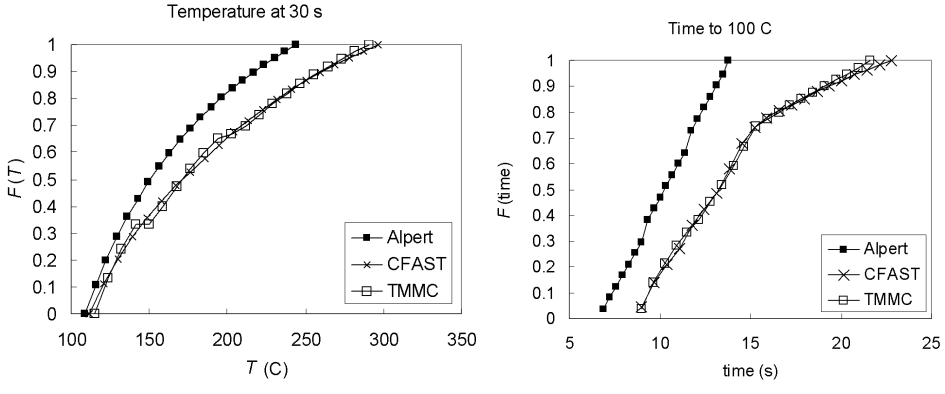


*Figure 3. Distributions of temperature at time = 30 s (left) and time to reach 100 °C (right) in the first validation test.*

The second validation test was the prediction of gas and heat detector temperatures in a room with concrete surfaces and predefined fire. In the test, CFAST two-zone model was used as Model A and FDS as Model B. The fire source was a rectangular burner at the floor level with maximum HRR per unit area of 700 kW/m$^2$. The co-ordinates and surface area of the fire source were random variables. In the beginning, the heat release rate increased proportional to $t^2$ reaching the final value at time $t_g$, which was a uniformly distributed

random variable. A list of the random variables is given in Table 1. The time to reach 200 °C at a certain location under the ceiling and the heat detector activation time were monitored.

*Table 1. Random variables in the second validation test.*

| Variable | Units | Distribution | Min | Max | Mean | Std.dev |
|---|---|---|---|---|---|---|
| BeamHeight $z_B$ | m | Uniform | 0.0 | 0.6 | | |
| GrowthTime $t_g$ | s | Uniform | 60.0 | 180.0 | | |
| Area | $m^2$ | Normal | 0.2 | 1.5 | 0.80 | 0.60 |
| FireX | m | Uniform | 0.0 | 4.0 | | |
| FireY | m | Uniform | 0 | 3.0 | | |

The predicted probability distributions for the time to reach a 200°C gas temperature are shown in Figure 4. As can be seen, the predictions using CFAST and FDS are considerably different: CFAST predicts that the 200°C temperature is reached in only 60% of the fires, but according to FDS the condition is met in 90% of fires. This makes the test very relevant and challenging.

The rank order correlations between the random variables and the time to reach the 200 °C gas temperature are shown in Figure 5. It demonstrates that in the cases where CFAST and FDS lead to different correlations, TMMC can make the necessary correction to the CFAST results.

The effect of the number of TMMC scaling points was studied by using different ways to divide the random space. The number of scaling points was varied from 1 to 32 and the basis for the division was taken from the CFAST simulations, which predicted that the fire surface area, the HRR growth time, and FireX-position were the most important random variables, as shown in Figure 5. The number of scaling points is denoted in the parentheses in Figure 4. For the case with 32 scaling points, a version with two scaling points per random variable (TMMC(32B)) was also tested ($2^5 = 32$).

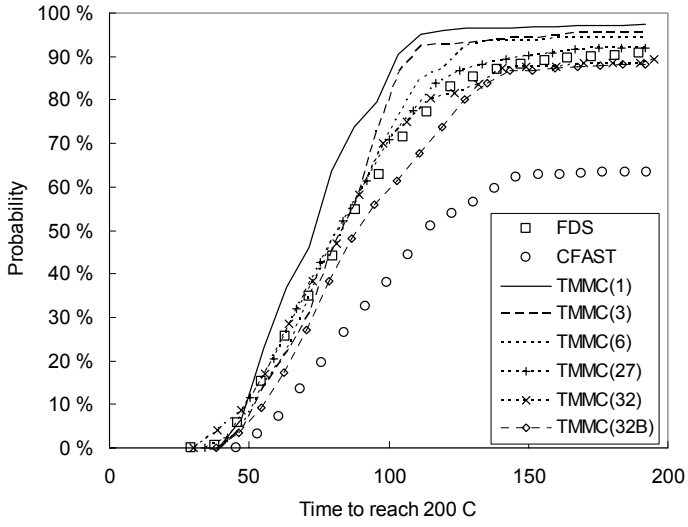


*Figure 4. Predicted probability distributions of time to reach 200 ℃ at gas in the second validation test.*

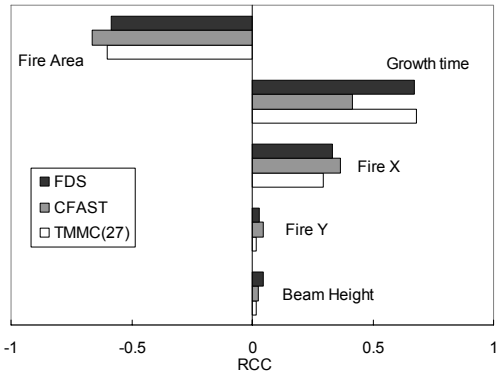


*Figure 5. Rank order correlation coefficients for the time to reach 200℃ gas temperature.*

The division of the random space has a clear effect on the accuracy of the TMMC distribution. If the division is made based on the relative importance of the random variables, the higher number of scaling points generally improves the accuracy. If the scaling points are chosen without any prior information of the importance, the results do not improve as much, as is demonstrated in the case TMMC(32B). In addition, smoothing the transient data was shown to improve the results.

The prediction of the heat detector activation time distribution was not as successful as the time to reach a certain gas temperature. The reason turned out to be the fact that in FDS, the heat detector temperature was not updated after the activation. An artificial limiter was thus applied to the model prediction, while the other model did not have such a limiter. In later versions of FDS, this feature has been changed accordingly, but the actual lesson learned from this exercise is that variables being scaled should rigorously represent the same physical quantity without any artificial limiters. If there is no correlation between the outputs of the two models, it does not make sense to scale one with another. Unfortunately, there is no simple way to identify the cases where this is not the case. The basic requirement for the TMMC applicability is that the relevant phenomena are included in both models at sufficient accuracy. In the validation tests above, both models had the necessary physics to describe the studied variables. Even though the zone and CFD models are mathematically very different, they both are theoretically capable of modelling the gas and heat detector temperatures within the fire room. However, trying to predict the vent mass flow using both ceiling jet correlation and zone model, for instance, would have been unsuccessful. In principle, the correlation between the two models can be ensured by computing a large number of model realizations with both models but in case of computationally expensive models like CFD, this is hardly practical. A good understanding of the behaviour of the physical models is therefore required for the judgement of the applicability of TMMC technique to the problem under consideration. Additionally, special attention should be paid to the choice of model B, since there is an inherent assumption that it is always more accurate than model A.

In the light of the above discussion, an important alternative for the use of totally different models than models A and B is the use of same model but with different numerical discretizations. The dependency of computational cost and accuracy of the CFD codes on the spatial resolution makes them suitable for the TMMC. The use of an FDS model in both phases of TMMC was demonstrated in [56]. Models A and B were FDS models with relatively coarse and fine computational meshes, respectively. When 1000 simulations were performed using model A and 24 simulations using model B, the savings in computation time was roughly a factor of five.

The results presented are special cases and do not prove that TMMC technique always works. However, the experiences so far have been positive, considering the improvement of both probabilities and correlations. This demonstrates the potential value of TMMC for large-scale quantitative fire risk studies in the future.

# Part II
# Radiative heat transfer solver for FDS fire model

# 4. Introduction

The quantitative risk analysis and performance-based design relies greatly on the use of numerical modelling and simulation of both the fire and evacuation processes. The increased size and complexity of the buildings make new demands for the techniques used for simulations. During the last few years, CFD has become the most widely used technique for the simulation of smoke transport and fire spread. The more simple techniques, such as the hand-calculation formulas and two-zone models, still have an important role in engineering because they are faster and simpler to use, but the majority of challenging fire simulations are performed using CFD. A literature review on CFD fire modelling is given in the next section.

Thermal radiation plays a very important role in the development of fires by allowing the gaseous combustion products to cool due to the emitted radiation and by preheating combustible materials ahead of the flame front. This preheating increases the rate of flame spread, often causing ignition of surfaces without direct flame impingement. Solution of the radiation transport equation requires determining radiative properties of the medium over a wide range of infrared frequencies. It is possible to create a radiation transport model that tracks the emission, transport, and absorption at many frequencies of infrared light. However, such an approach is very time consuming and memory intensive. One typical simplification is to assume a grey gas and solve for only one integrated intensity. The presence of condensed phase particles or droplets can block thermal radiation and thus reduce the rate of fire spread. To incorporate the effect of radiation-spray interaction to the model, the radiative properties of the spray must be calculated with the same level of detail as the gas phase, and the scattering effects must be considered.

The Fire Dynamics Simulator (FDS), developed at the National Institute of Standards and Technology (NIST), originally used a simple Monte Carlo ray tracing method for solving the transport of heat by radiation from the combustion region to the surroundings. This model was easy to implement and worked well for small fires. However, the model did not function well for large fires or fires approaching flashover, and a new radiation heat transfer solver was based on the finite volume method for radiation [57], as described in the papers III–V of the thesis.

# 5. Fire modelling using Computational Fluid Dynamics

## 5.1 Scope of the review

The purpose of this section is to review the aspects of the physical and numerical modelling in the present CFD fire models. The emphasis is put on the physical issues such as fluid dynamics, combustion, radiation, solid phase heat transfer, flame spread and two-phase flows. The features of LES and RANS models and the challenges of radiation modelling are discussed in detail. The issues of numerical implementations and user interfaces are shortly discussed. The models designed for some special types of applications, such as explosions or Direct Numerical Simulation of combustion processes are not discussed.

In 2002 SFPE Handbook chapter concerning the CFD Fire Modelling, Cox and Kumar [58] presented the principles, practices and instruction for proper use of CFD in fire applications, from the perspective of Reynolds-averaged Navier-Stokes (RANS) technique. When the chapter was written, it was widely accepted that the proper method for low speed turbulent flow was RANS using an eddy viscosity turbulence model such as the $k$-ε model, SIMPLE pressure correction algorithm [59] or some of its variants, and the various sub-models like Eddy Break-Up [60] for combustion. However, in a few years, due to faster computers and specialized algorithms, Large Eddy Simulation (LES) is now considered by many to be the preferable technique to study fire-driven flows. LES technique is used in Fire Dynamics Simulator (FDS) [61, 62], which was made publicly available in the year 2000. For FDS users, the article of Cox and Kumar provides very little guidance, although there is no fundamental difference between RANS and LES, other than the treatment of time dependence of the Navier-Stokes equations. This example illustrates how rapidly a computational field of engineering may evolve.

The CFD fire models can be classified based on many different criteria, with RANS vs. LES being probably the most widely used. Other possibilities would be the type of radiation model, availability, price, user interface and hardware requirement. All these aspects have been discussed in the review article of Olenick and Carpenter [63].

## 5.2 Physical models

### 5.2.1 Fluid dynamics

The core of any CFD model is its Navier-Stokes solver. The numerical solution of these equations is considered by many to be a "mature" field because it has been practised for over 30 years, but the nature of turbulence is still one of the unsolved problems of physics. All the current solvers are based on the approximations that have effects on the applicability of the solver and the accuracy of the results – also in the fire simulations.

Current, practical CFD fire models fall into one of two major categories: Reynolds-averaged Navier-Stokes (RANS) or Large Eddy Simulation (LES). The difference of these two categories is the nature of the starting equations: In RANS, the Navier-Stokes equations are *time* or *ensemble averaged* before the derivation of the discrete form suitable for programming as a solver algorithm. The solver then finds a *steady state* or *quasi steady state* solution for the equations. Time dependent flows can be solved as long as the time scale of the mean flow is large compared to the time scale of the turbulent fluctuations [64]. In LES, the time averaging is not performed, and the solutions can be considered "accurate" in time, meaning that the variations in the solution correspond to the motions resolvable by the numerical grid. The marching in time takes place using a short time step $\Delta t$, which is usually defined by the following stability criteria

$$\Delta t < \min_{ijk}\left(\Delta x_{ijk} / u_{ijk}\right) \tag{7}$$

where $\Delta x$ and $u$ are the grid cell size and velocity, respectively, and the minimum is found over the whole domain. Equation (7) is called Courant-Friedrichs-Lewy (CFL) condition [65, 66] according to the German mathematicians who invented it in 1928 – well before modern computers. In LES, the filtering is performed in space, although the actual filtering is usually limited to the length scales below the grid cell size.

The difference of the RANS and LES results is depicted in Figure 6 showing the temperature fields of a pool fire flame. While the RANS result shows smooth

variations and looks like a laminar flame, the LES result clearly illustrates the large scale eddies. Both results are correct solutions of the corresponding equations. However, the time accuracy of LES is also essential for the quantitative accuracy of the buoyancy driven flows. As the NIST researches Rehm and Baum have shown [67], the dynamic motions or 'eddies' are responsible for most of the air entrainment into the fire plumes. Since these motions can not be captured by RANS, LES is usually better suited for fire-driven flow. LES typically requires a better spatial resolution than RANS. Examples of RANS-based fire CFD codes are JASMINE, KAMELEON [68], SMARTFIRE [69], SOFIE [70], ISIS [71] and ISIS-3D [72]. Examples of LES codes are the FDS [61, 62]; SMAFS, developed at Lund University [73]; and the LES fire code developed at the City University of Hong Kong [74].

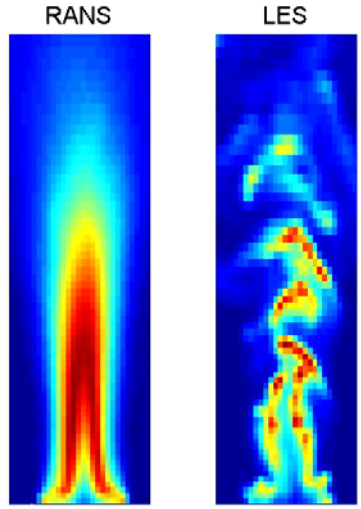


*Figure 6. A comparison of temperature fields in a pool fire flame simulations using RANS and LES.*

There are certain applications, where RANS has a clear advantage over LES. RANS models can take advantage of any a priori knowledge of the mean flow direction by accepting high aspect ratio grid cells. An example of such an application is a flow in a tunnel, where the grid cells can be made long and thin, giving good accuracy in the direction normal to the tunnel walls but saving cells in the direction of the tunnel, where variations are slow. In LES, all the velocity components are present with likelihood of same order, and the cell aspect ratios

must be close to unity. For this reason, the tunnel simulations using LES are computationally expensive. The second type of application where the use of RANS is advantageous is the simulation of long, close to steady state or steady state fires. In such cases, RANS allows fast marching in time using long time steps, while LES is bound by the CFL condition.

Turbulence modelling and time accuracy are closely related. In RANS solvers, the turbulence models are used to describe all the turbulent properties of the flow. A range of different models have been developed. The differences in the models have been mainly related to the assumption of homogenous ($k$-$\varepsilon$, $k$-$\omega$) or inhomogeneous (Reynolds stress models) turbulence and the treatment of boundary layers (Wall functions vs. Small Reynolds Number models). The problems of these models to accurately predict the entrainment of buoyant plumes has been known for long, and is more fundamental than just turbulence closure problem. A review of the turbulence modelling in RANS is given by Kumar [75], and the effect of turbulence models on the CFD simulation of buoyant diffusion flames has been studied by, for example, Liu and Wen [76].

In LES, the role of turbulence models is only to describe the sub-grid scale phenomena that cannot be solved with the computational grid used. In regions of high shear, the sub-grid scale models have a stronger effect on the solution and a lot of research is still needed to find good solutions for handling these flows. Examples of high shear flows in fire simulations are the solid wall boundaries and the interface of the hot and cold flows in doors and windows.

Despite the relatively short history of LES fire modelling, the accuracy of LES technique in fire simulation has been studied extensively. Early validation of FDS predecessor was performed by comparing simulations against salt water experiments [77, 78, 79], fire plumes [80, 81] and room fires [82]. More recently, FDS code has been validated for fire plumes [83] and fires in enclosures in the context of the World Trade Center investigation [84, 85] and the fire model validation project sponsored by the U.S. Nuclear Regulatory Commission [86].

Virtually all CFD fire models assume incompressible flow, which is adequate in typical fire application, but should be kept in mind when dealing with high velocity cases and explosions. Inclusion of the compressibility effects in fire simulations would increase the computational cost considerably. One of the few

compressible fire codes is the Uintah Computational Framework developed at C-SAFE project of the University of Utah [87].

In RANS simulations, the boundary layers have traditionally been handled using the wall functions which assume the logarithmic velocity profile on the wall. In simple applications of the process industry, these functions work well, having the most serious problems in situations involving separation and reattachment. Similar "sub-grid scale wall functions" can be derived for LES, or the effect of the wall can be taken into account in the sub-grid scale model of viscosity [88]. Currently, FDS does not include any wall functions. Only an adjustment of the slip-velocity and simple heat transfer coefficient correlations are used. In their comparison of measured and predicted turbulence statistics, Zhang et al. [89] showed that even with these simple boundary treatments, FDS was able to produce good flows in a room scale. Naturally, new techniques must be studied to improve the accuracy of solid phase heat transfer and flame spread predictions.

### 5.2.2 Combustion

The most important difference between the majority of the CFD applications and the fire CFD is what drives the flow. In typical non-fire CFD, the boundary conditions such as inflow velocity drive the flow. Fire problems, in turn, are always driven by the combustion source terms. The accuracy of the combustion model is therefore essential for the quality of the whole simulation.

Fire science has always been a small field compared to combustion science, which is clearly the closest relative. Through the history of fire CFD, the combustion models have been developed for other combustion problems and directly applied to fire problems. For almost 20 years, the eddy break-up (EBU) or eddy dissipation models were the standard. With the EBU, in its simplest form, the local rate of fuel consumption is calculated as [60]

$$R_{FU} = \overline{\rho}\frac{\varepsilon}{k}\min\left[C_R m_{fu}, \frac{C'_R m_{ox}}{s}\right] \tag{8}$$

where $\varepsilon$ and $k$ are the turbulent diffusivity and energy, respectively; $m_{fu}$ and $m_{ox}$ are the time averaged mass fractions of fuel and oxidant, respectively; $s$ denotes

the stoichiometric oxygen to fuel mass ratio and $C_R$ and $C''_R$ are empirical constants. The form of EBU expression is based mainly on dimensional arguments. Ratio $k/\varepsilon$ is the turbulent time scale. If the turbulence intensity is high, so is the fuel consumption. For the prediction of secondary species, like CO and HCl, and soot, more advanced models based on the laminar flamelets have been used [90].

In LES, it is obvious that the EBU type of model cannot be used because the turbulence quantities are not calculated. The models developed by the combustion scientists for LES are usually based on the use of flamelets and rely on good spatial accuracy where both temperature and concentration fields are well captured in the vicinity of the reaction zone. From this starting point, the range of possible physical models is only limited by the imagination of the engineers or mathematicians and the requirement of computational efficiency. In a typical fire simulation, neither the temperature nor the species concentrations are accurately captured. The robustness can thus only be achieved by simplicity.

In FDS, a relatively simple flame sheet model, presented in Paper III of the thesis, has been used. The local heat release rate is based on the mass loss rate of oxygen that is computed from the mixture fraction diffusion across the flame surface using the following formula:

$$\dot{m}''_{O_2} = -\frac{dY_{O_2}}{dZ}\rho D \nabla Z \cdot \vec{n}\Big|_{Z=Z_f} \tag{9}$$

where $Y_{O2}$ is the oxygen mass fraction, $D$ is the diffusion coefficient and $\vec{n}$ is the flame surface normal. The derivative of the oxygen mass fraction, $dY_{O2}/dZ$, depends only on the assumed chemical reaction. The model has performed very well for most fire scenarios but has had problems capturing some of the more complicated phenomena, such as under-ventilated fires and local ignition and extinction. An extension of the single-scalar mixture fraction model to a two- or three-scalar version has been made in the latest version of FDS [61] in order to capture these effects. The use of laminar flamelet combustion models within FDS have been studied by Yang et al. [91] and Kang & Wen [92]. Unfortunately, the performance or advantage over the simple flame-sheet model in large-scale fire simulation was not demonstrated in these studies. In large-scale calculations, the mixture fraction and temperature fields close to the flame sheet have

overshoots, caused by the second-order transport scheme. It is still unclear how the laminar flamelet models that require both second and first moments of the local mixture fraction field could work in this situation.

### 5.2.3 Radiation

In enclosure fires, radiation may be the dominating mode of heat transfer. For flames burning in an open atmosphere, the radiative fraction of overall heat transfer ranges from less than 0.1 up to 0.4, depending both on the fuel type and the fire diameter [93]. Due to the important role that the radiation plays in fires, all the fire CFD models have a radiation model that solves the radiation transport equation (RTE) [94, 95]

$$\underbrace{\mathbf{s}\cdot\nabla I_\lambda(\mathbf{x},\mathbf{s})}_{\text{rate of change}} = -\underbrace{\left[\kappa_\lambda(\mathbf{x})+\sigma_\lambda(\mathbf{x})\right]I_\lambda(\mathbf{x},\mathbf{s})}_{\text{rate of attenuation}} + \underbrace{\kappa_\lambda(\mathbf{x})I_b(\mathbf{x},\lambda)}_{\text{esmission source}} + \underbrace{\frac{\sigma_\lambda(\mathbf{x})}{4\pi}\int_{4\pi}\Phi(\mathbf{s},\mathbf{s}')I_\lambda(\mathbf{x},\mathbf{s}')d\Omega'}_{\text{in-scattering}} \tag{10}$$

where $\mathbf{s}$ is the unit direction vector; $I_\lambda$ is the intensity at wavelength $\lambda$; $\kappa_\lambda(\mathbf{x})$ and $\sigma_\lambda(\mathbf{x})$ are the local absorption and scattering coefficients at $\lambda$, respectively; $I_b$ is the emissive power of the medium; $\Phi(\mathbf{s},\mathbf{s}')$ is the scattering phase function giving the scattered intensity from direction $\mathbf{s}'$ to $\mathbf{s}$. The terms of the RTE have the following interpretations: The left hand side is the rate of change of the intensity in direction $\mathbf{s}$; the first right hand side term describes the attenuation by absorption and scattering to other directions; the second right hand side term is the emission source term; the last right hand side term is the in-scattering integral, describing how much intensity is gained by scattering from all the other directions to the present direction. The intensity depends on place, direction and wavelength. Typically, the wavelength dependence is removed by first integrating the RTE over the spectrum, and solving RTE for the integrated field.

Like combustion modelling, the development of radiation modelling in fire CFD has consisted mostly of the copying of techniques developed for combustion simulations. However, in fires the radiation modelling may be even more challenging and its role more pronounced than in the pure combustion problems.

A wide range of different radiation models have been used for fire CFD over the years. The models mainly differ from each other in the way how they solve the spatial and angular field of intensity. The simple models like P-1 and six flux models [94] were popular in the early years. In P-1, the diffusion approximation of RTE is adopted, and spherical harmonics are used to describe the intensity. It is best suited for optically thick cases where intensity fields are fairly smooth. The six-flux model in turn is related to the use of Cartesian grid system; the intensity is solved in the six co-ordinate directions. The ray tracing models such as Discrete Transfer (DT) [96] are theoretically good for fires but may become computationally expensive. In DT, RTE is integrated along the imaginary lines of sight, or rays, starting from the boundaries of the domain. The flux models like Discrete Ordinates Methods (DOM) [95] and Finite Volume Method (FVM) [57] are currently the most popular in new codes. In these models, the solid angle is first divided to small control angles or directions, and the flux of intensity for each direction is solved separately in space. DOM and FVM are very similar techniques. In DOM, the angular distributions are defined by generalized $S_N$ and $T_N$ quadratures. In FVM, the polar/azimuthal discretization is code specific but the angular integration is performed exactly. The most general technique is the use of Monte Carlo where the radiative emission and absorption processes are modelled by sending photons with random energy and direction. It is currently beyond the computational resources in most practical simulations, but an important validation tool for the other models. However, MC can be used if the spatial resolution of the simulation is very coarse, in which case the total number of photons does not increase too much. Various modelling approaches for radiative heat transfer in pool fires are compared in [97].

Another feature of RTE that needs modelling is the calculation of the absorption coefficient $\kappa(\mathbf{x},\lambda)$, which depends on the local gas and soot concentrations. In a typical fire CFD, a grey gas is assumed, which means that a single value is used for the whole spectrum. Some aspects of the spectral resolution can be captured by dividing the spectrum to a relatively small number of bands, and solving a separate RTE for each band. In the combustion literature, a large number of wide-band models have been developed to account for the band-structure of the emission spectra of the most important combustion gases. The most accurate results could be obtained by using a narrow-band model, where separate RTEs are solved for hundreds of wavelengths. This is still too expensive for practical

fire CFD. The use of correlated-*k* [98] and spectral narrow-band and global gas radiation models [99, 100] have been studied at Kingston University.

Next, some of the challenges of radiation modelling are discussed:

i. **Inhomogeneity**: The strong inhomogeneity of the optical properties and temperature field makes the simplest and fastest models like P-1 and six flux models very inaccurate. The presence of large optically thin areas aggravates the ray effect for all the models dealing with discrete directions, especially the ray tracing methods.

ii. **Emission source term**: For spectrally integrated RTE, the emission source term is

$$\kappa I_b = \kappa T^4 \tag{11}$$

where $T$ is the local temperature. Due to the $T^4$-dependence, it is extremely sensitive to errors in temperature. For example, a 15% underestimation of temperature would lead to a source term that is 48% too small. In large-scale simulation, this kind of error in the flame region can rarely be avoided. The problem is typically solved by modelling the emission term either as a linear function of heat release rate (used in FDS) or using precomputed flamelet libraries (e.g. SOFIE).

iii. **Spectral dependence**: Ways to handle the spectral dependence of the radiation are currently being studied to find computationally efficient ways to include both the smooth emission spectrum from soot and solid surfaces, and the sharp peaks of gaseous combustion products.

iv. **Time dependence**: The inherent time dependence of the fires sets strong requirements for the computational efficiency. In RANS codes, the radiation field must be updated within the internal iterations of the time step, but the computational cost can be relaxed by solving RTE only every *N*th iteration. In SOFIE, for example, it is typical to use $N$=10. In FDS, the time accuracy of the radiation field has been relaxed by solving the FVM equations typically every third time step and only part of the directions at the time.

v. **Scattering**: When the beam of radiation meets soot or water droplets, it is scattered to all directions. The scattering has a tremendous effect on the radiation blocking ability of the fine water sprays and smoke. Due to the computational complexity, scattering has often been neglected in fire CFD codes. To accurately simulate the water mist and sprinkler systems, this effect should be taken into account. There are actually two challenges related to the scattering: The first challenge is the computation of the radiative properties, i.e. absorption and scattering coefficients and the scattering phase function. For water droplets, Mie-theory can be used for the calculation of *single droplet* radiative properties. Free subroutines performing these Mie-calculations are available for use in the radiation solvers [101, 102]. The integration over the spectrum and droplet size distribution must be performed in the model. The second challenge is the computation of the scattering integral. The first approximation is to use isotropic scattering, which considerably simplifies the computation. Full integrations using DOM and FVM have been performed in simplified scenarios [103, 104, 105], but not yet in practical fire CFD. In FDS, the scattering integral is approximated by a combination of functions describing isotropic and forward scattering, as explained in Paper V of this thesis and summarized in Section 6.2.5.

vi. **Soot**: In fires, soot is usually the most important source and absorber of radiation. The modelling of soot formation and oxidation processes is therefore important for the accurate prediction of radiation emissions. Detailed models that solve the fields of soot number density and mass fraction have been developed over the years, and implemented also in fire CFD codes such as SOFIE, and more recently in [106] and [107]. In post-flame conditions, the problem is mostly following of the soot produced in the flame zone. Currently, FDS can only follow this "inactive" soot, but an attempt to include more advanced soot modelling was presented by Lautenberger et al. [108]. Unfortunately, the soot formation and oxidation processes are sensitive to the temperature and the same problems appear as in the detailed modelling of combustion.

### 5.2.4 Solid phase heat transfer

The solution of solid phase heat transfer is needed in the analysis of structures response to fires and the simulation of flame spread on solid surfaces. The solution of this conjugate heat transfer problem is typical for fires but rarely found from commercial CFD packages. Over the years, different techniques have been developed to tackle this problem. Since the solid phase heat transfer is a completely separate problem from the fluid dynamics problem, the following techniques are code specific, having no relation to the use of RANS or LES.

i. The simplest technique is to use separate numerical solvers for the fluid and solid phases and to exchange information through the boundary conditions. The use of separate solver allows a flexible gridding inside the solid phase, which is required due to the three orders of magnitude in thermal conductivities. It is also easy to include various physical phenomena like charring and moisture transfer. Quite often, one-dimensional solution of the heat conduction equation on each wall cell is accurate enough. This technique is implemented as an internal subroutine for FDS.

ii. Separate solvers of three-dimensional heat conduction can be linked to the CFD solver, either as an external code (e.g. KAMELEON) or internal subroutine (SOFIE). Specialized algorithms may be needed to model the connection between the gas and solid phases due to the disparity in length and time scales [109]. In the recent ECSC project concerning the CFD modelling of natural fires (*The development and validation of a CFD-based engineering methodology for evaluating thermal action on steel and composite structures, co-ordinated by BRE, UK*), a three-dimensional heat conduction model was developed for SOFIE code. The model allows the simulation of temperature profiles in structural metal elements such as beams and columns. The information between the fluid and solid phases is passed through the boundary conditions, and fine structural gridding can be used. The solver requires a special user interface developed by BRE (UK) and is limited to I-shape structures.

iii. A full coupling of the solid and fluid phases can be achieved by solving only one enthalpy equation, common for both phases. Such an approach was used in SOFIE code [70], but the use of a structured grid system

usually prevented the necessary refinement inside the solids. A fully coupled system is being developed in the C-SAFE project at University of Utah [87]. However, the practical applications of this code have not been demonstrated, probably due to the extremely high computational cost of the solver.

### 5.2.5 Flame spread

The simulation of flame spread is one of the most challenging and most important physical modelling problems in fire CFD. The importance is caused by the need to simulate fire development instead of fire consequences. The challenge comes from the fact that in order to simulate the flame spread process, one must be able to simulate all three sub-processes:

i. The development of far field temperature and radiation. In large fires, the far field radiation dominates the heat transfer.

ii. The flame structure and heat transfer in the region close to the wall. In small fires, the near field flames are responsible for most of the heat transfer to the wall. In a typical fire simulation, this region is totally covered by one or two grid cells, making it impossible to capture the flame structure and temperature distribution. Some kind of sub-grid scale model of this region is needed in fire CFD codes to accurately model the flame spread. The sub-grid scale model might use the ideas of wall functions and boundary layer flame structures [110].

iii. The heat transfer and pyrolysis inside the solid material.

In the context of fire CFD, the flame spread simulation usually means the ability to predict the fire growth starting from a *small initial fire* or ignition point, where all three sub-processes are important but the second sub-process dominates the heat transfer. The fire spread, in turn, means the ignition of solid surfaces in the presence of a relatively *large initial fire* dominating the heat transfer by radiation. In practice, the small and large initial fires should be defined relative to the CFD mesh: A large initial fire spans from 10 to 20 grid cells, for example. Currently, none of fire CFD codes can reliably predict the flame spread, with the exception of some relatively simple cases. The reason is

the inability to capture the near wall phenomena, as explained above. Despite this fact, fire spread simulations are routinely performed.

### 5.2.6 Multiple phases

The transport of water droplets can be simulated with practically all the fire CFD codes. The level of detail may vary, but the basics of the mass and heat transfer can be handled. Monodisperse droplets have traditionally been assumed by the two-phase solvers, but in fires, it is important to include the whole size distribution of droplets, because the different droplet sizes have very different effects in the fire: large droplets transport most of the water mass and have a sufficient momentum to penetrate the buoyant flow. Small droplets in turn block radiation more efficiently than large droplets. The evaporation of droplets is important to include for the simulation of the gas phase suppression effects. Far more difficult than the actual modelling is to find good boundary conditions for water nozzles. Surprisingly little data has been published on the droplet size and velocity distributions of common sprinkler or water mist nozzles. To some extent, the uncertainty of droplet size distributions can be reduced by modelling the secondary droplet breakup mechanism [110], i.e. by trying to predict the stable droplet size of the water jet. Various models for droplet breakup and coalescence were summarized by Madsen [112].

## 5.3 Numerical implementations

The efficiency and robustness of the numerical implementation is often equally or even more important than the sophistication of the physical models. For academic purposes, the implementation of the most elaborate physical models may be justified, but quite often the resulting code is of little use for fire engineering. The requirement of computational efficiency is even more pronounced when CFD is used as a tool of probabilistic analysis, as discussed in Part I of the thesis.

Most fire CFD codes use structured meshes; some of them curvilinear and some Cartesian. The advantage of the Cartesian mesh is the simplicity of the solver, which often leads to fast computing and reduced risk of coding errors. The

obvious weakness is the difficulty of describing complex geometries. To overcome this, methods such as cut-cell method have been developed [113] Naturally, there are cases where the geometry could be much more efficiently described by curved structured or unstructured mesh. Therefore, the comparison of various codes based on some individual property is not justified. The most important question is: "Which code gives the required answer with lowest cost and sufficient reliability?" The cost naturally includes both the price of the software and the required hardware, but also the required working time and learning.

A common way to add some flexibility to the structured and Cartesian solvers is the so-called multi-block technique, where the solution domain is divided to individual blocks having a their own computational grids. The availability of low-cost personal computers and the possibility to build small computer clusters has increased the interest in the parallel processing which is often based on the domain decomposition where each block is associated with its own processor. This parallelisation technique has the following advantages: (1) It is relatively easy to implement, although the efficient communications need careful organisation of the data structures. (2) It can be very efficient when the individual blocks share only a small amount of common information. The natural boundaries of the fire scenario, such as walls and floors, should be used as block boundaries whenever possible. The disadvantages of this technique include: (1) The possibility of instability, especially in LES, if the block boundaries are out of phase. (2) The difficulty of load balancing.

## 5.4 User interfaces

The quality of the user interface has been claimed to be crucial for the reliability and usability of fire CFD codes. From this perspective, it has been quite surprising to see the success of FDS, having originally no user interface at all for input. Lately, such an user interface has become available as a commercial software [114]. Naturally, the availability of a good post processing tool has been crucial for the FDS success. One reason for the emphasis on (graphical) user interfaces may have been the large number of controlling parameters in the RANS codes. These parameters have a strong effect on the convergence of the solver, but are difficult to understand by ordinary users. In engineering applications with complicated geometries and high requirements for efficiency, a

well-designed graphical user interface may help to avoid user errors by giving instant visual feedback. At best, the interface guides the user through the modelling process thus reducing the need to remember the meanings of the input parameters and syntaxes and therefore improving the modelling reliability.

Several challenges are associated with the development of the graphical user interfaces: (1) They must be maintained parallel with the actual solver, and this may be more laborious than the solver development. (2) It may be difficult to select which features of the CFD code should be available in the user interface and which should not. (3) So far, the tools of 3D geometry definition are neither versatile nor easy to use. In most cases, it is faster to write the definition in a simple text file than create the three-dimensional drawing. Tools that use CAD and other building design information may change the situation in the future. Automatic generation of FDS models from a building product model has been studied in [115] and [116].

# 6. Development of the radiation solver

## 6.1 Radiative transport equation

The radiative transport equation (RTE) for spectral intensity $I_\lambda$ passing through a participating medium is [94, 95]

$$\frac{1}{c}\frac{\partial I_\lambda(\mathbf{x},\mathbf{s},t)}{\partial t} + \mathbf{s}\cdot\nabla I_\lambda(\mathbf{x},\mathbf{s},t) = -\left[\kappa_\lambda(\mathbf{x}) + \sigma_\lambda(\mathbf{x})\right] I_\lambda(\mathbf{x},\mathbf{s},t) + B_\lambda(\mathbf{x},t) + \frac{\sigma_\lambda(\mathbf{x})}{4\pi}\int_{4\pi}\Phi(\mathbf{s},\mathbf{s}')I_\lambda(\mathbf{x},\mathbf{s}',t)d\Omega' \tag{12}$$

For most engineering applications, the time derivative can be neglected because of the large magnitude of $c$. If we assume that a local thermodynamic equilibrium is established and that the Kirchoff's law is valid, the emission term $B_\lambda(\mathbf{x},t)$ is related to the Planck function

$$B_\lambda(\mathbf{x},t) = \kappa_\lambda(\mathbf{x}) I_{\lambda b}(T) = \kappa_\lambda(\mathbf{x})\frac{e_{\lambda b}(T)}{\pi} \tag{13}$$

The RTE for absorbing-emitting and scattering medium can now be written as

$$\underbrace{\mathbf{s}\cdot\nabla I_\lambda(\mathbf{x},\mathbf{s})}_{\text{rate of change}} = \underbrace{-\left[\kappa_\lambda(\mathbf{x}) + \sigma_\lambda(\mathbf{x})\right] I_\lambda(\mathbf{x},\mathbf{s})}_{\text{rate of attenuation}} + \underbrace{\kappa_\lambda(\mathbf{x}) I_{\lambda b}(\mathbf{x})}_{\text{esmission source}} + \underbrace{\frac{\sigma_\lambda(\mathbf{x})}{4\pi}\int_{4\pi}\Phi(\mathbf{s},\mathbf{s}')I_\lambda(\mathbf{x},\mathbf{s}')d\Omega'}_{\text{in-scattering}} \tag{14}$$

where the temperature dependence of the Planck function is implicit through the position vector **x**. In a non-scattering case, the RTE simplifies to

$$\mathbf{s}\cdot\nabla I_\lambda(\mathbf{x},\mathbf{s}) = \kappa_\lambda(\mathbf{x})\left[I_{\lambda b}(\mathbf{x}) - I_\lambda(\mathbf{x},\mathbf{s})\right] \tag{15}$$

## 6.2 Model formulation

This section describes the approximations and assumptions that are made during the development of the numerical radiation transport solver in FDS. The general description and applications of the Finite Volume radiation solver were provided in papers III and IV of the thesis. Paper V described the model for radiation-water spray interaction. Section 7 summarizes the results of two verification tests, also available in the FDS (version 5) User's guide [62] and the validation tests originally presented in papers IV and V.

### 6.2.1 Spectrally averaged RTE

In practical fire simulations, the spectral (λ) dependence of thermal radiation cannot be solved accurately. Instead, the radiation spectrum can be divided into a relatively small number of wavelength bands and a separate RTE is derived for each band. For a non-scattering gas, the band specific RTE is

$$\mathbf{s}\cdot\nabla I_n(\mathbf{x},\mathbf{s}) = \kappa_n(\mathbf{x})\left[I_{nb}(\mathbf{x}) - I_n(\mathbf{x},\mathbf{s})\right], \qquad n = 1...N \tag{16}$$

where $I_n$ is the intensity integrated over the band $n$, and $\kappa_n$ is the appropriate mean absorption coefficient within the band. The source term can be written as a fraction of the blackbody radiation

$$I_{nb} = F_n \frac{\sigma T^4}{\pi} \tag{17}$$

where $\sigma$ is the Stefan-Boltzmann constant. $F_n$ is defined as

$$\begin{aligned} F_n = F_{\lambda_{\min}-\lambda_{\max}} &= F_{0-\lambda_{\max}} - F_{0-\lambda_{\min}} = F_{0-\lambda_{\max}T} - F_{0-\lambda_{\min}T} \\ &= \frac{1}{\sigma}\left[\int_0^{\lambda_{\max}T} \frac{e_{\lambda b}(\lambda,T)}{T^5}\,d(\lambda T) - \int_0^{\lambda_{\min}T} \frac{e_{\lambda b}(\lambda,T)}{T^5}\,d(\lambda T)\right] \end{aligned} \tag{18}$$

where $\lambda_{\min}$ and $\lambda_{\max}$ are the lower and upper bounds of the wavelength band, respectively [94]. $F_{0\text{-}\lambda T}$ can be written as an infinite series [117]

$$F_{0-\lambda T} = \frac{15}{\pi^4} \sum_{j=1}^{\infty} \frac{e^{-jz}}{j} \left( z^3 + \frac{3z^2}{j} + \frac{6z}{j^2} + \frac{6}{j^3} \right) \tag{19}$$

where $z = C_2/\lambda T$ and $C_2$ is the Planck's second radiation constant. In FDS, 50 terms are used in the series to compute $F_{0-\lambda T}$. The values of $F_{0-\lambda T}$ are tabulated in the range $0 < \lambda T < 10^5$ μmK with 25 μmK intervals. During the simulation, the values of $F_n$ are found by table-lookup using the band limits and local temperature.

When the intensities corresponding to the bands are known, the total intensity is calculated by summing over all the bands

$$I(\mathbf{x},\mathbf{s}) = \sum_{n=1}^{N} I_n(\mathbf{x},\mathbf{s}) \tag{20}$$

Even with a reasonably small number of bands, solving multiple RTEs is very time consuming. Fortunately, in most large-scale fire scenarios, soot is the most important combustion product controlling the thermal radiation from the fire and hot smoke. As the radiation spectrum of soot is continuous, it is possible to assume that the gas behaves as a grey medium. The spectral dependence is then lumped into one absorption coefficient ($N = 1$) and the source term is given by the blackbody radiation intensity

$$I_b = \frac{\sigma T^4}{\pi} \tag{21}$$

This is the default mode of FDS and appropriate for most problems of fire engineering. In optically thin flames, where the amount of soot is small compared to the amount of $CO_2$ and water, the grey gas assumption may produce significant overpredictions of the emitted radiation. From a series of numerical experiments it has been found that six bands ($N = 6$) are usually enough to improve the accuracy in these cases. The limits of the bands are selected to give an accurate representation of the most important radiation bands of $CO_2$ and water. If the absorption of the fuel is known to be important, separate bands can be reserved for fuel, and the total number of bands is increased to nine ($N = 9$).

For simplicity, the fuel is assumed to be $CH_4$. The limits of the bands are shown in Table 2.[2]

*Table 2. Limits of the wavelength bands in both wave numbers ($\nu$) and wave lengths ($\lambda$).*

| 9 Band Model | 1 | 2 | 3 | 4 | 5 | 6 | 7 | 8 | 9 |
|---|---|---|---|---|---|---|---|---|---|
| Major Species | Soot | $CO_2$ $H_2O$, Soot | $CH_4$ Soot | Soot | $CO_2$ Soot | $H_2O$ | $H_2O$ $CH_4$, Soot | Soot | Soot |
| $\nu$ (1/cm) | 10000 | 3800 | 3400 | 2800 | 2400 | 2174 | 1429 | 1160 | 1000 | 50 |
| $\lambda$ (μm) | 1.00 | 2.63 | 2.94 | 3.57 | 4.17 | 4.70 | 7.00 | 8.62 | 10.0 | 200 |

| 6 Band model | 1 | 2 | 3 | 4 | 5 | 6 |
|---|---|---|---|---|---|---|
| Major Species | Soot | $CO_2$ $H_2O$, Soot | $CH_4$ Soot | $CO_2$ Soot | $H_2O$, $CH_4$, Soot | Soot |

For the calculation of the grey or band-mean absorption coefficients, $\kappa_n$, a narrow-band model, RadCal [118], has been implemented in FDS. At the start of a simulation, the absorption coefficients are tabulated as a function of mixture fraction and temperature. During the simulation, the local absorption coefficient is found by table-lookup.

In calculations of limited spatial resolution, the source term, $I_b$, in the RTE requires special treatment. In the neighbourhood of the flame sheet, both temperatures and absorption coefficient are smeared out over a grid cell and are thus considerably lower than one would expect in a diffusion flame. Because of its fourth-power dependence on the temperature, the source term must be modelled in those grid cells cut by the flame sheet. Elsewhere, there is greater confidence in the computed temperature, and the source term can be computed directly

[2] The presented band structure corresponds to version 5 of FDS [61]. Slightly different band limits were used in the pool fire simulations in Paper II.

$$\kappa I_{nb} = \begin{cases} F_n \kappa \sigma T^4 / \pi & \text{Outside flame zone} \\ F_n \max\left(\chi_r \dot{q}''' / 4\pi, \kappa \sigma T^4 / \pi\right) & \text{Inside flame zone} \end{cases} \tag{22}$$

Here, $\dot{q}'''$ is the chemical heat release rate per unit volume and $\chi_r$ is an empirical estimate of the *local* fraction of that energy emitted as thermal radiation. For a small fire ($D$ < 1 m), the local $\chi_r$ is approximately equal to its global counterpart. However, as the fire increases in size, the global value will typically decrease due to the net absorption of the thermal radiation by the increasing smoke mantle.

The boundary condition for the radiation intensity leaving a diffuse wall is given as

$$I_{nw}(\mathbf{s}) = F_n \frac{\varepsilon \sigma T_w^4}{\pi} + \frac{1-\varepsilon}{\pi} \int_{\mathbf{s}'\cdot\mathbf{n}<0} I_{nw}(\mathbf{s}') |\mathbf{s}' \cdot \mathbf{n}| d\mathbf{s}' \tag{23}$$

where $I_w(\mathbf{s})$ is the intensity at the wall, $\varepsilon$ is the mean hemispherical emissivity, and $T_w$ is the wall surface temperature. The walls are assumed to behave as diffuse reflectors when $\varepsilon$ < 1.

The radiant heat flux vector is defined as

$$\dot{\mathbf{q}}''(\mathbf{x}) = \int_{4\pi} \mathbf{s}' I(\mathbf{x}, \mathbf{s}') d\mathbf{s}' \tag{24}$$

and the total combined intensity as

$$U(\mathbf{x}) = \sum_{n=1}^{N} \int_{4\pi} I_n(\mathbf{x}, \mathbf{s}') d\mathbf{s}' \tag{25}$$

The radiative loss term in the gas phase energy equation is

$$-\nabla \cdot \dot{\mathbf{q}}_r''(\mathbf{x})(\text{gas}) = \kappa(\mathbf{x})\left[U(\mathbf{x}) - 4\pi I_b(\mathbf{x})\right] \tag{26}$$

In words, the net radiant energy gained by a control volume is the difference between that which is absorbed and that which is emitted.

### 6.2.2 Discretized RTE

The radiative transport equation (16) is solved using techniques similar to those for convective transport in finite volume methods for fluid flow [57], thus the name given to it is the Finite Volume Method (FVM). Note that the procedure outlined below is appropriate for each band of a wide band model, thus the subscript *n* has been removed for clarity.

To obtain the discretized form of the RTE, the unit sphere is divided into a finite number of solid angles. In each grid cell, a discretized equation is derived by integrating equation over the volume of cell *ijk* and the control angle $\partial\Omega^l$, to obtain

$$\int_{\partial\Omega}\int_{V_{ijk}} \mathbf{s}\cdot\nabla I(\mathbf{x}',\mathbf{s}')d\mathbf{x}'d\mathbf{s}' = \int_{\partial\Omega^l}\int_{V_{ijk}} \kappa(\mathbf{x}')\left[I_b(\mathbf{x}') - I(\mathbf{x}',\mathbf{s}')\right]d\mathbf{x}'d\mathbf{s}' \tag{27}$$

The volume integral on the left-hand side is replaced by a surface integral over the cell faces using the divergence theorem. Assuming that the radiation intensity $I(\mathbf{x},\mathbf{s})$ is constant on each of the cell faces, the surface integral can be approximated by a sum over the cell faces. Assuming further that $I(\mathbf{x},\mathbf{s})$ and $\kappa(\mathbf{x})$ are constants within the volume $V_{ijk}$ and over the angle $\partial\Omega^l$ we obtain

$$\sum_{m=1}^{6} A_m I^l_{ijk,m}\int_{\partial\Omega^l}(\mathbf{s}'\cdot\mathbf{n}_m)d\mathbf{s}' = \kappa_{ijk}\left[I_{b,ijk} - I^l_{ijk}\right]V_{ijk}\partial\Omega^l \tag{28}$$

where

| | |
|---|---|
| $I^l_{ijk}$ | is the radiant intensity in direction $\mathbf{s}^l$ in cell *ijk* |
| $I^l_{ijk,m}$ | is the radiant intensity in direction $\mathbf{s}^l$ at face *m* of cell *ijk* |
| $I_{b,ijk}$ | is the radiant source term in the cell *ijk* |
| $\partial\Omega^l$ | is the solid angle centred around the direction vector $\mathbf{s}^l$ |
| $V_{ijk}$ | is the volume of cell *ijk* |
| $A_m$ | is the area of cell face *m* of cell *ijk* |
| $\mathbf{n}_m$ | is the unit normal vector of the cell face *m* of cell *ijk.* |

Note that while the intensity is assumed constant within the angle $\partial\Omega^l$, its direction covers the angle $\partial\Omega^l$ exactly.

In Cartesian coordinates, the normal vectors $\mathbf{n}_m$ are the base vectors of the coordinate system. As a result, the integrals over the solid angle do not depend on the physical coordinate, but the direction only, and can be calculated analytically. Equation (28) can be simplified to

$$a_{ijk}^{l} I_{ijk}^{l} = a_{x}^{l} I_{xu}^{l} + a_{y}^{l} I_{yu}^{l} + a_{z}^{l} I_{zu}^{l} + b_{ijk}^{l} \tag{29}$$

where

$$a_{ijk}^{l} = A_x \left| D_x^l \right| + A_y \left| D_y^l \right| + A_z \left| D_z^l \right| + \kappa_{ijk} V_{ijk} \delta\Omega^l \tag{30}$$

$$\begin{aligned} a_x^l &= A_x \left| D_x^l \right| \\ a_y^l &= A_y \left| D_y^l \right| \\ a_z^l &= A_z \left| D_z^l \right| \end{aligned} \tag{31}$$

$$b_{ijk}^{l} = \kappa_{ijk} I_{b,ijk} V_{ijk} \delta\Omega^l \tag{32}$$

$$\delta\Omega^l = \int_{\Omega^l} d\Omega = \int_{\delta\phi\delta\theta} \int \sin\theta d\theta d\phi \tag{33}$$

$$\begin{aligned} D_x &= \int_{\Omega^l} \left( \mathbf{s}^l \cdot \mathbf{i} \right) d\Omega \\ &= \int_{\delta\phi\delta\theta} \int \left( \mathbf{s}^l \cdot \mathbf{i} \right) \sin\theta d\theta d\phi \\ &= \int_{\delta\phi\delta\theta} \int \cos\phi \sin\theta \sin\theta d\theta d\phi \\ &= \frac{1}{2} \left( \sin\phi^+ - \sin\phi^- \right) \left[ \Delta\theta - \left( \cos\theta^+ \sin\theta^+ - \cos\theta^- \sin\theta^- \right) \right] \end{aligned} \tag{34}$$

$$
\begin{aligned}
D_y &= \int_{\Omega^l} \left(\mathbf{s}^l \cdot \mathbf{j}\right) d\Omega \\
&= \int_{\delta\phi\delta\theta} \int \sin\phi \sin\theta \sin\theta d\theta d\phi \\
&= \frac{1}{2}\left(\cos\phi^- - \cos\phi^+\right)\left[\Delta\theta - \left(\cos\theta^+ \sin\theta^+ - \cos\theta^- \sin\theta^-\right)\right]
\end{aligned}
\tag{35}
$$

$$
\begin{aligned}
D_z &= \int_{\Omega^l} \left(\mathbf{s}^l \cdot \mathbf{k}\right) d\Omega \\
&= \int_{\delta\phi\delta\theta} \int \cos\theta \sin\theta d\theta d\phi \\
&= \frac{1}{2}\Delta\phi\left(\sin^2\theta^+ - \sin^2\theta^-\right)
\end{aligned}
$$

Here **i**, **j** and **k** are the base vectors of the Cartesian coordinate system. $\theta^+$, $\theta^-$, $\phi^+$ and $\phi^-$ are the upper and lower boundaries of the control angle in the polar and azimuthal directions, respectively, and $\Delta\theta = \theta^+ - \theta^-$ and $\Delta\phi = \phi^+ - \phi^-$. The solution method of equation (29) is based on an explicit marching sequence [119]. The marching direction depends on the propagation direction of the radiation intensity. As the marching is done in the "downwind" direction, the "upwind" intensities in all three spatial directions are known, and the intensity $I^l_{ijk}$ can be solved directly from an algebraic equation. This makes the numerical solution of the FVM very fast. Iterations are needed only to account for the reflective boundaries, optically very thick scenarios and scattering. In practice, no iterations are made in FDS because the frequency of radiation solutions is quite high due to the small time step of the LES flow solver, and the time accuracy of the radiative heat fluxes is sufficient for engineering purposes. Some degree of delay between the flow and radiation solutions is accepted.

### 6.2.3 Spatial and angular discretization

The grid used for the RTE solver is the same as for the fluid solver. The rectangular domain is divided into rectangular grid cells. Each cell is assigned indices *i*, *j* and *k*, representing the position of the cell in *x*, *y* and *z* directions, respectively.

The coordinate system used to discretize the solid angle is shown in Figure 7. The discretization of the solid angle is done by dividing first the polar angle, θ, into $N_\theta$ bands, where $N_\theta$ is an even integer. Each θ-band is then divided into $N_\phi(\theta)$ parts in the azimuthal (ϕ) direction. $N_\phi(\theta)$ must be divisible by 4. The numbers $N_\theta$ and $N_\phi(\theta)$ are chosen to give the total number of angles $N_\Omega$ as close to the value defined by the user as possible. $N_\Omega$ is calculated as

$$N_\Omega = \sum_{i=1}^{N_\theta} N_\phi(\theta_i) \tag{36}$$

The distribution of the angles is based on empirical rules that try to produce equal solid angles $\delta\Omega^l = 4\pi/N_\Omega$. The number of θ-bands is

$$N_\theta = 1.17 N_\Omega^{1/2.26} \tag{37}$$

rounded to the nearest even integer. The number of ϕ-angles on each band is

$$N_\phi(\theta_i) = \max\left\{4, \frac{N_\Omega}{2}\left[\cos(\theta_i^-) - \cos(\theta_i^+)\right]\right\} \tag{38}$$

rounded to the nearest integer that is divisible by 4. $\theta^-$ and $\theta^+$ are the lower and upper bounds of the θ-band, respectively. The discretization is symmetric with respect to the planes $x = 0$, $y = 0$, and $z = 0$. This symmetry has three important benefits: First, it avoids the problems caused by the fact that the first-order upwind scheme, used to calculate intensities on the cell boundaries, is more diffusive in non-axial directions than axial. Second, the treatment of the mirror boundaries becomes very simple. Third, it avoids the so-called "overhang" situations, where **s'·i**, **s'·j** or **s'·k** would change sign inside the control angle. These "overhangs" would make the resulting system of linear equations more complicated. In the axially symmetric case, these "overhangs" can not be avoided, and a special treatment, developed by Murthy and Mathur [120], is applied. In these cases, $N_\phi(\theta)$ is kept constant, and the total number of angles is $N_\Omega = N_\theta \times N_\phi$. In addition, the angle of the vertical slice of the cylinder is chosen to be the same as $\Delta\phi$.

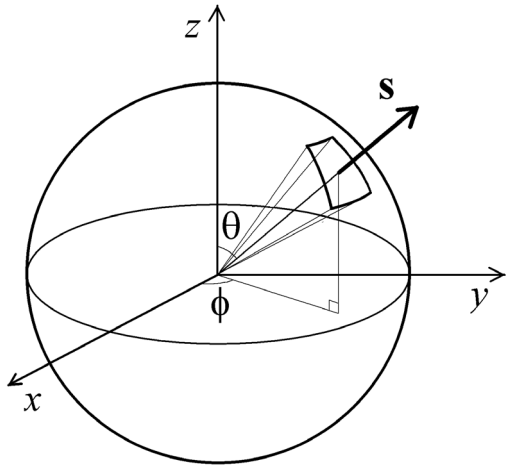


*Figure 7. The discretization of the angular direction in FVM for radiation.*

### 6.2.4 Computation of cell face intensities

To close the system described by equation (29), the cell face intensities $I^l_{ijk,m}$ must be computed. Several alternatives have been proposed, but the FVM does not constrain this choice provided that conservation is rigorously maintained [121]. To illustrate some typical schemes to compute the cell face intensities, let us consider the situation shown in Figure 8. The task is to solve the intensity $I^l$ to the direction $\mathbf{s}^l$ at cell *ijk* when the value of $I^l_{(i-1)jk}$ in the cell (*i*-1)*jk* is known. The intensity at the cell face between (*i*-1)*jk* and *ijk* is $I^l_u$.

If the intensity $I^l_{(i-1)jk}$ is written as a weighted sum of cell face intensities

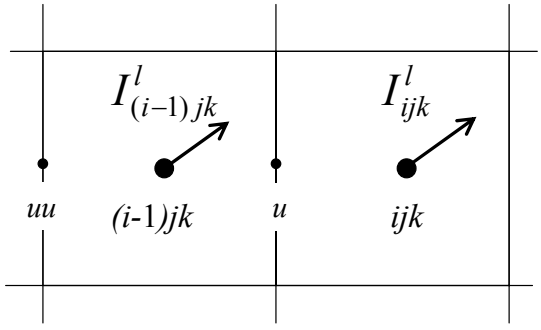


*Figure 8. The notation of cell face intensities.*

$$I^l_{(i-1)jk} = fI^l_u + (1-f)I^l_{uu} \tag{39}$$

we can solve

$$I^l_u = \left[I^l_{(i-1)jk} - (1-f)I^l_{uu}\right]/f \tag{40}$$

The simplest possible approximation is $f$ = 1. In the numerical heat transfer literature, the resulting scheme is called the *step scheme*:

$$I^l_u = I^l_{(i-1)jk} \tag{41}$$

The step scheme is first order accurate in space, and is sometimes referred to as the *upwind scheme*. It is very fast to compute, since the cell face intensities are directly taken from the upstream solutions. A scheme of second-order accuracy is obtained by setting $f$ = 0.5. The resulting scheme is called *diamond scheme*

$$I^l_u = 2I^l_{(i-1)jk} - I^l_{uu} \tag{42}$$

The diamond scheme is supposed to be more accurate than the step scheme, but like the higher-order schemes in fluid dynamics, it may become unstable in some situations. As a result, the intensities may have positive and negative spikes or unphysical values like $I^l_u < 0$. The diamond scheme requires more memory than the step scheme because the intensities $I^l_{uu}$ must also be stored.

Even higher accuracy can be achieved by the use of exponential schemes where the development of intensity inside the grid cells is computed using the Beer-Lambert law. The *modified exponential scheme* of Chai et al. [122] is formulated as

$$I^l_u = I^l_{(i-1)jk} e^{-\kappa\Delta x} + I_{b,ijk}\left(1 - e^{-\kappa\Delta x}\right) \tag{43}$$

where $\Delta x$ is the distance that the intensity has travelled within cell ($i$-1)$jk$. The schemes based on the use of exponential functions may have much higher computing times than the schemes based on simple algebraic operations.

In FDS code, the cell face intensities are computed using the first-order step scheme. The advantage of the lower order accuracy is that the ray effect is actually reduced due to the numerical diffusion. This phenomenon is illustrated in Figure 9 showing the total combined intensity around a methane flame. The step scheme was used in the figure on the left and diamond scheme in the figure on the right. The intensity field of the step scheme is more uniform than the intensity of the diamond scheme, which clearly shows the directions of angular discretization.

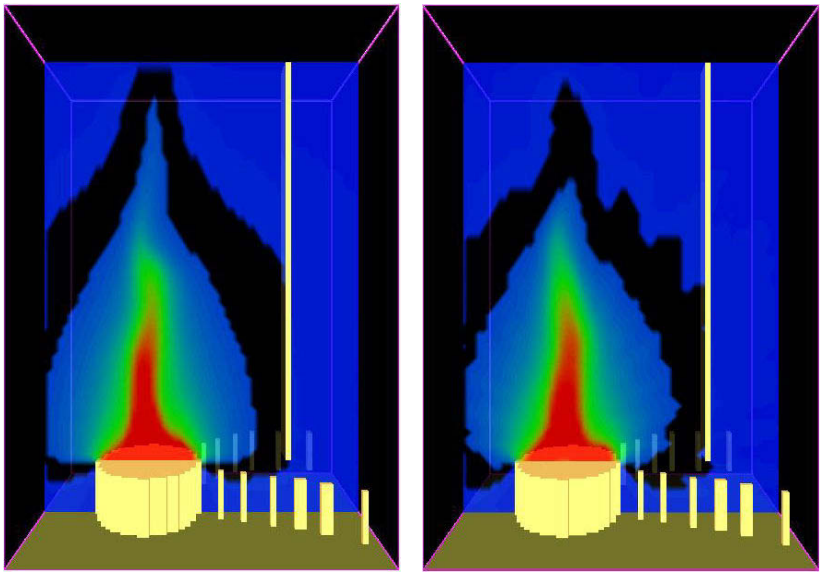

*Figure 9. Effect of intensity interpolation schemes on ray effect. The step scheme is on the left and the diamond scheme is on the right.*

### 6.2.5 Interaction between liquid sprays and radiation

The attenuation of thermal radiation by liquid droplets is an important consideration, especially for water mist systems [123]. Liquid droplets attenuate thermal radiation through a combination of scattering and absorption. The radiation-droplet interaction must therefore be solved for both the accurate prediction of the radiation field and for the droplet energy balance.

The situation of radiation-spray interaction is illustrated in Figure 10. Intensity $I_\lambda(\mathbf{s})$ is entering to a grid cell containing liquid droplets with size distribution

$f(r,\mathbf{x})$. The mass of liquid within the cell is $\rho_d(\mathbf{x})\ V_{ijk}$. Some part of the energy is scattered to an angle $\theta_d$ from the original direction. The scattering is assumed to be axially symmetric around the initial direction.

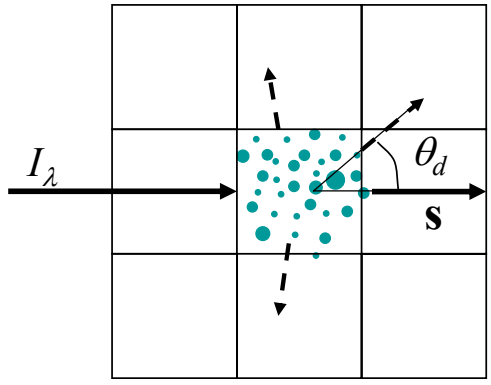


*Figure 10. The radiation-droplet interaction.*

If the gas phase absorption and emission are temporarily neglected for simplicity, the radiative transport equation (14) becomes

$$\mathbf{s}\cdot\nabla I_\lambda(\mathbf{x},\mathbf{s}) = -\left[\kappa_{\lambda,d}(\mathbf{x})+\sigma_{\lambda,d}(\mathbf{x})\right] I_\lambda(\mathbf{x},\mathbf{s}) + \kappa_{\lambda,d}(\mathbf{x}) I_{b\lambda,d}(\mathbf{x}) + \frac{\sigma_{\lambda,d}(\mathbf{x})}{4\pi}\int_{4\pi}\Phi(\mathbf{s},\mathbf{s}')I_\lambda(\mathbf{x},\mathbf{s}')d\Omega' \tag{44}$$

where $\kappa_{\lambda,d}$ and $\sigma_{\lambda,d}$ are the droplet absorption and scattering coefficients at wavelength $\lambda$, respectively, and $I_{\lambda b,d}$ is the emission term of the droplets. $\Phi(\mathbf{s},\mathbf{s}')$ is a scattering phase function that gives the scattered intensity from direction $\mathbf{s}'$ to $\mathbf{s}$. The local absorption and scattering coefficients are calculated from the local droplet number density $N(\mathbf{x})$ and mean diameter $d_m(\mathbf{x})$ as

$$\kappa_{\lambda,d}(\mathbf{x}) = N(\mathbf{x})\int_{r=0}^{\infty} f(r,d_m(\mathbf{x}))C_a(r,\lambda)dr$$
$$\sigma_{\lambda,d}(\mathbf{x}) = N(\mathbf{x})\int_{r=0}^{\infty} f(r,d_m(\mathbf{x}))C_s(r,\lambda)dr \tag{45}$$

where $r$ is the droplet radius and $C_a$ and $C_s$ are absorption and scattering cross sections, respectively. The droplet number density function $f(r,d_m)$ is assumed to have the same form as the initial droplet size distribution, but a mean diameter depending on the location **x**. For the numerical implementation, the above equations are written in the form

$$\kappa_{\lambda,d}(\mathbf{x}) = A_d(\mathbf{x}) \int_{r=0}^{\infty} \frac{f(r,d_m(\mathbf{x}))C_a(r,\lambda)}{\pi\left[d_m(\mathbf{x})/2\right]^2} dr$$
$$\sigma_{\lambda,d}(\mathbf{x}) = A_d(\mathbf{x}) \int_{r=0}^{\infty} \frac{f(r,d_m(\mathbf{x}))C_d(r,\lambda)}{\pi\left[d_m(\mathbf{x})/2\right]^2} dr \tag{46}$$

where $A_d$ is the total cross sectional area per unit volume of the droplets. $A_d$ is approximated as

$$A_d(\mathbf{x}) \approx \frac{\rho_d(\mathbf{x})}{2\rho_w d_m(\mathbf{x})/3} \tag{47}$$

where $\rho_w$ is the density of liquid water. An accurate computation of the in-scattering integral on the right hand side of equation (44) would be extremely time consuming. It is here approximated by dividing the total $4\pi$ solid angle to a "forward angle" $\delta\Omega^l$ and "ambient angle" $\delta\Omega^* = 4\pi - \delta\Omega^l$ . For compatibility with the FVM solver, $\delta\Omega^l$ is set equal to the control angle given by the angular discretization. However, it is assumed to be symmetric around the centre of the control angle. Within $\delta\Omega^l$ the intensity is $I^l(\mathbf{x},\mathbf{s})$ and elsewhere it is approximated as

$$U_\lambda^*(\mathbf{x}) = \frac{U_\lambda(\mathbf{x}) - \delta\Omega^l I_\lambda(\mathbf{x})}{\delta\Omega^*} \tag{48}$$

where $U_\lambda(\mathbf{x})$ is the combined intensity at wavelength $\lambda$. The in-scattering integral can now be written as

$$\frac{\sigma_{\lambda,d}(\mathbf{x})}{4\pi} \int_{4\pi} \Phi(\mathbf{s},\mathbf{s}') I_\lambda(\mathbf{x},\mathbf{s}') d\Omega' = \sigma_{\lambda,d}(\mathbf{x})\left[\chi_f I_\lambda(\mathbf{x},\mathbf{s}) + (1-\chi_f)U^*(\mathbf{x})\right] \tag{49}$$

where $\chi_f \equiv \chi_f(r,\lambda)$ is a fraction of the total intensity originally within the solid angle $\delta\Omega^l$ that is scattered into the same angle $\delta\Omega^l$. A derivation of the formula for $\chi_f$ in case of two-flux approximation has been presented in Ref. [124]. For an arbitrary solid angle it becomes

$$\chi_f(r,\lambda) = \frac{1}{\delta\Omega^l}\int_0^{\mu^l}\int_0^{\mu^l}\int_{\mu_{d,0}}^{\mu_{d,\pi}} \frac{P_0(\mu_d)}{\left(1-\mu^2\right)\left(1-\mu'^2\right)-\left(\mu_d-\mu\mu'\right)}\, d\mu_d\, d\mu\, d\mu' \tag{50}$$

where $\mu_d = \cos\theta_d$ and $P_0(\mu_d)$ is a single droplet scattering phase function

$$P_0(\mu_d) = \frac{\lambda^2\left(\left|S_1(\mu_d)\right|^2 + \left|S_2(\mu_d)\right|^2\right)}{2C_s(r,\lambda)} \tag{51}$$

$S_1(\mu_d)$ and $S_2(\mu_d)$ are the two polarized scattering amplitudes, given by Mie-theory. The integration limit $\mu^l$ is a cosine of the polar angle defining the boundary of the symmetric control angle $\delta\Omega^l$

$$\mu^l = \cos(\theta^l) = 1 - \frac{2}{N_\Omega} \tag{52}$$

The limits of the innermost integral are

$$\begin{aligned} \mu_{d,0} &= \mu\mu^l + \sqrt{1-\mu^2}\sqrt{1-\mu'^2} \\ \mu_{d,\pi} &= \mu\mu^l - \sqrt{1-\mu^2}\sqrt{1-\mu'^2} \end{aligned} \tag{53}$$

When $\chi_f$ is integrated over the droplet size distribution to get an averaged value, it is multiplied by $C_s(r,\lambda)$. It is therefore $|S_1|^2 + |S_2|^2$, not $P_0(\mu_d)$, that is integrated. Physically, this means that intensities are added, not probabilities [125].

An effective scattering coefficient can now be defined

$$\overline{\sigma}_{\lambda,d}(\mathbf{x}) = \frac{4\pi N(\mathbf{x})}{4\pi - \delta\Omega^l}\int_0^\infty (1-\chi_f)C_s(r,\lambda)\,dr \tag{54}$$

and the spray RTE becomes

$$\mathbf{s}\cdot\nabla I_{\lambda}(\mathbf{x},\mathbf{s}) = -\left[\kappa_{\lambda,d}(\mathbf{x}) + \overline{\sigma}_{\lambda,d}(\mathbf{x})\right] I_{\lambda}(\mathbf{x},\mathbf{s}) + \kappa_{\lambda,d}(\mathbf{x}) I_{b\lambda,d}(\mathbf{x}) + \frac{\overline{\sigma}_{\lambda,d}(\mathbf{x})}{4\pi} U_{\lambda}(\mathbf{x}) \tag{55}$$

This equation can be integrated over the spectrum to get the band specific RTEs. The procedure is exactly the same as that used for the gas phase RTE. After the band integrations, the spray RTE for band *n* becomes

$$\mathbf{s}\cdot\nabla I_{n}(\mathbf{x},\mathbf{s}) = -\left[\kappa_{n,d}(\mathbf{x}) + \overline{\sigma}_{n,d}(\mathbf{x})\right] I_{n}(\mathbf{x},\mathbf{s}) + \kappa_{n,d}(\mathbf{x}) I_{bn,d}(\mathbf{x}) + \frac{\overline{\sigma}_{n,d}(\mathbf{x})}{4\pi} U_{n}(\mathbf{x}) \tag{56}$$

where the source function is based on the average droplet temperature within a cell. The droplet contribution to the radiative loss is

$$-\nabla\cdot\dot{\mathbf{q}}''_{\mathrm{r}}(\mathbf{x})(\text{droplets}) = \kappa_{d}(\mathbf{x})\left[U(\mathbf{x}) - I_{b,d}(\mathbf{x})\right] \tag{57}$$

For each individual droplet, the radiative heating/cooling power is computed as

$$\dot{q}_{\mathrm{r}} = \frac{m_{d}}{\rho_{d}(\mathbf{x})}\kappa_{d}(\mathbf{x})\left[U(\mathbf{x}) - I_{b,d}(\mathbf{x})\right] \tag{58}$$

where $m_d$ is the mass of the droplet and $\rho_{\mathrm{d}}(\mathbf{x})$ is the total density of droplets in the cell.

The absorption and scattering cross sections and the scattering phase functions are calculated using the MieV code developed by Wiscombe [125]. Currently, the spectral data on is only included for water. The values of the imaginary part of the complex refractive index (absorption coefficient) are taken from Ref. [126], and value 1.33 is used for the real part (index of refraction).

Before the actual simulation, both $\kappa_d$ and $\sigma_d$ are averaged over the possible droplet radii and wavelength. A constant "radiation" temperature, $T_{\mathrm{rad}}$, is used in the wavelength averaging. $T_{\mathrm{rad}}$ should be selected to represent a typical radiating

flame temperature. By default, $T_{rad}$ = 1173 K. After the averaging processes, the spray radiative properties are functions of the mean droplet diameter only. The properties are computed for a range of different mean diameters and stored in one-dimensional arrays. During the simulation, the local properties are found by table look-up using the local mean droplet diameter.

# 7. Results

## 7.1 Verification of the radiation solver

The purpose of the computer program verification is to ensure that the program works as intended by the developers and indicated by the program documentation. The verification cases are typically simpler than the actual applications of the program. The verification may have some features of validation, if the verification includes assessment of the accuracy of the results.

The first verification test is the computation of the configuration factors within a rectangular enclosure with one hot wall and other walls maintained at 0 K, shown in Figure 11. The enclosure dimensions are chosen to be that of a cube. The exact values of the configuration factor from plane element *dA* to parallel rectangle *H* are calculated using the analytical solution [94]. Different variations of the case are generated by varying the mesh resolution ($20^3$ and $100^3$ cells) and the number of radiation angles (50, 100, 300, 1000, 2000). A comparison of the exact solutions and FDS predictions at different positions at the diagonal are shown in Figure 12. As can be seen, the FDS predictions converge towards the exact solution when *both* spatial *and* angular resolutions are improved.

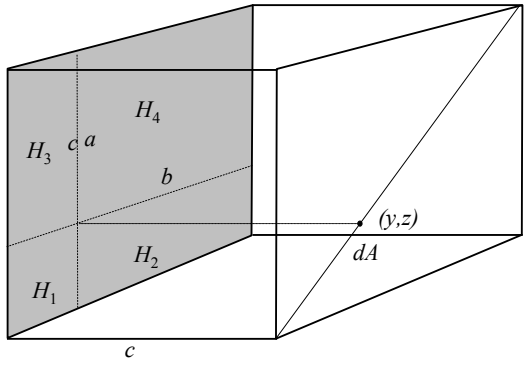


*Figure 11. Radiation verification test for configuration factor computation.*

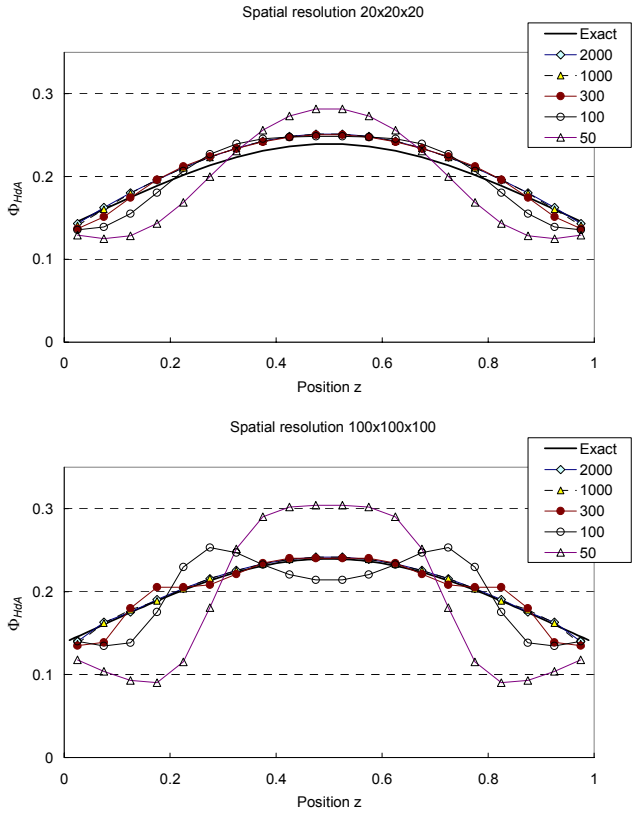


*Figure 12. Comparison of exact configuration factors to FDS predictions with different angular resolutions and two different spatial resolutions. Top: 20 × 20 × 20, bottom: 100 × 100 × 100.*

The second verification test is a three-dimensional computation of the radiative heat flux from a 1.0 m thick homogenous layer of grey and stagnant gas between black infinitely wide walls. The range of optical thicknesses is studied by varying the absorption coefficient $\kappa$. The gas temperatures $T_g$ = 1273.15 K and wall temperatures $T_{w1} = T_{w2} = 0$ K. In a special case with non-absorbing gas ($\kappa = 0$), the temperature of the opposite wall is $T_{w1}$ = 1273.15 K. The exact solution [127] for the heat flux to wall 2 is given by

$$S(\kappa) = \begin{cases} \sigma T_g^4 \left[1 - 2E_3(\kappa L)\right] & \kappa > 0 \\ T_{w1}^4 & \kappa = 0 \end{cases} \tag{59}$$

where $L$ = 1.0 m. The FDS results are computed at two mesh resolutions (I = 20 and I = 150 cells) in the direction over the layer. For the smaller resolution, both one-band and six-band results are included to test the integration of heat fluxes over multiple bands. Two-dimensional versions are also computed (J = 1). The number of radiation angles was 104. The exact values and the FDS predictions are shown in Table 3.

*Table 3. The solutions for the radiative flux from a plane layer.*

| $\kappa$ (m$^{-1}$) | S ($\kappa$) | FDS 3D (I = 20) | | FDS 2D (I = 20) | | FDS 3D (I = 150) |
|---|---|---|---|---|---|---|
| | | 1-band | 6-band | 1-band | 6-band | |
| 0 | 149 | 149 | 148 | 148 | 147 | 149 |
| 0.01 | 2.90 | 2.92 | 2.91 | 2.84 | 2.83 | 2.93 |
| 0.1 | 24.9 | 25.6 | 25.5 | 25.1 | 25.0 | 25.7 |
| 0.5 | 82.9 | 83.1 | 82.8 | 84.4 | 84.1 | 84.0 |
| 1.0 | 116 | 115 | 115 | 118 | 117 | 117 |
| 10.0 | 149 | 149 | 148 | 149 | 148 | 149 |

## 7.2 Radiative fluxes from diffusion flames

The accuracy of the predicted radiative heat fluxes from methane pool flames was studied in Paper IV. Methane and natural gas fires were established in a quiescent environment using circular burners with diameters 0.10 m, 0.38 m and 1.0 m. Radiometers were used to measure the radial and vertical profiles of radiative heat flux outside the flame. A schematic diagram of the set-up is shown in Figure 13 and the experimental approach is reported in Ref. [128]. The radiative flux typically drops off very quickly in the radial direction, whereas in the vertical direction, the flux peaks at a vertical location equal to approximately 50% of the characteristic flame height and then drops to small values above the visible flame tip. The uncertainty (with a coverage factor of two) in the radiative flux measurement is estimated as 10%.

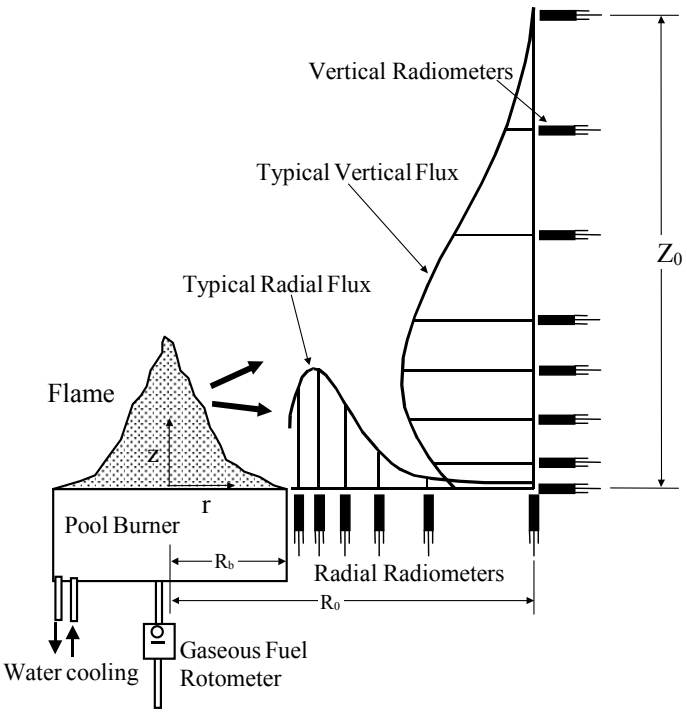


*Figure 13. Experimental set-up for measurement of radiative flux.*

The parameters of the simulated cases are summarized in Table 4, where $D$ is the burner diameter, $R_0$ is the radial position of the vertical row of radiometers, $\dot{m}''_F$ is the mass burning rate per burner area and $\dot{Q}''$ is the rate of heat release per burner area. The size of the simulation domain and the size of the computational grid cell just above the burner surface, $\delta x$, are also shown. The last two columns show the dimensionless heat release rates $Q_D^* = \dot{Q}/(\rho_\infty T_\infty c_p D^2 \sqrt{gD})$ [55] and $Q_{\delta x}^* = \dot{Q}''/(\rho_\infty T_\infty c_p D^2 \sqrt{g\delta x})$ where $\rho_\infty$, $T_\infty$ and $c_p$ are the properties of the ambient air. $Q_D^*$ is the standard dimensionless number, which characterizes the strength of the fire and $Q_{\delta x}^*$ represents the resolution of the current grid, in proportion to the burning rate. A very low value of $Q_{\delta x}^*$ indicates that the position of the flame near the burner surface cannot be resolved. 304 radiation angles were used. A soot conversion factor of 1.0% was assumed for all calculations.

The predictions for the radiative fractions of the heat release rate were systematically higher than the measurements, probably due to the overestimation of the flame temperatures. The measured and predicted radial distributions of

radiative flux are compared in Figure 14. The agreement is very good in general, but the heat flux is highly over estimated in cases B and E. Similar trends can be found in Figure 15, showing the vertical profiles. A few remarks should be made when interpreting the results. First, high radiative fluxes were predicted better than low fluxes, which is good for the applicability in safety relevant scenarios. Second, the 100% errors in radiative heat flux may be caused by as low as 20% error in absolute temperature. The reason for the large error in case B, where the flame should be relatively well resolved, is currently not known.

*Table 4. Summary of the simulated methane / natural gas experiments.*

| Case | Test configuration | | | | Simulated domain | Simulation parameters | | |
|---|---|---|---|---|---|---|---|---|
| | $D$ (m) | $R_0$ (m) | $\dot{m}''_F$ (g/m$^2$/s) | $\dot{Q}''$ (kW/m$^2$) | x × y × z (m$^3$) | $\delta x$ (cm) | $Q_D^*$ | $Q_{\delta x}^*$ |
| A | 0.10 | 0.82 | 1.08 | 53.8 | 0.315 × 0.21 × 0.45 | 0.525 | 0.12 | 0.67 |
| B | 0.10 | 0.82 | 4.80 | 240 | 0.315 × 0.21 × 0.45 | 0.525 | 0.53 | 3.0 |
| C | 0.38 | 0.732 | 5.90 | 295 | 1.26 × 0.84 × 1.80 | 2.1 | 0.34 | 1.8 |
| D | 0.38 | 0.732 | 31.0 | 1550 | 1.26 × 0.84 × 2.20 | 2.1 | 1.8 | 9.6 |
| E | 1.0 | 1.00 | 1.25 | 62.4 | 2.50 × 2.00 × 3.50 | 5.0 | 0.044 | 0.31 |
| F | 1.0 | 0.80 | 4.12 | 206 | 2.50 × 2.00 × 4.50 | 5.0 | 0.14 | 1.05 |

## 7.3 Attenuation of radiation in water sprays

Two validation tests were presented in Paper V. The first validation test is the simulation of an experiment conducted by Murrel et al. [129]. They measured the attenuation of thermal radiation passing through a water spray using a heat flux gauge. The schematics of the system are shown in Figure 16. The radiation was produced by a 1 m × 1 m heat panel at 900°C. Three different nozzles were simulated. Each nozzle was a full-cone type industrial nozzle. The simulations were performed at eight different flow rates for each nozzle.

The initial droplet size distribution was assumed to have the following cumulative distribution for droplet diameter $d$

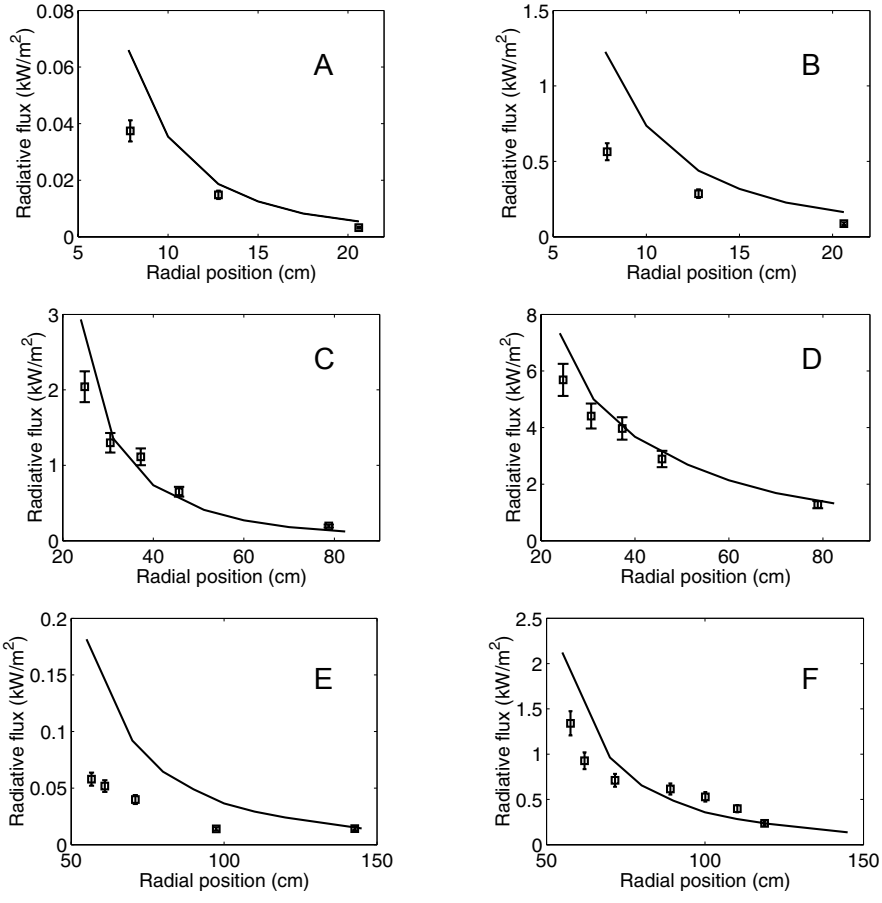


*Figure 14. Comparison of the measured (squares) and predicted (lines) radial heat flux distributions.*

$$F(d)=\begin{cases}\dfrac{1}{\sqrt{2\pi}}\displaystyle\int_0^d \frac{1}{\sigma\tau}\exp\left\{\frac{-\left[\ln\left(\tau/d_m\right)\right]^2}{2\sigma^2}\right\}d\tau & (d\le d_m)\\ 1-\exp\left[-0.693\left(\dfrac{d}{d_m}\right)^{\gamma}\right] & (d>d_m)\end{cases} \tag{60}$$

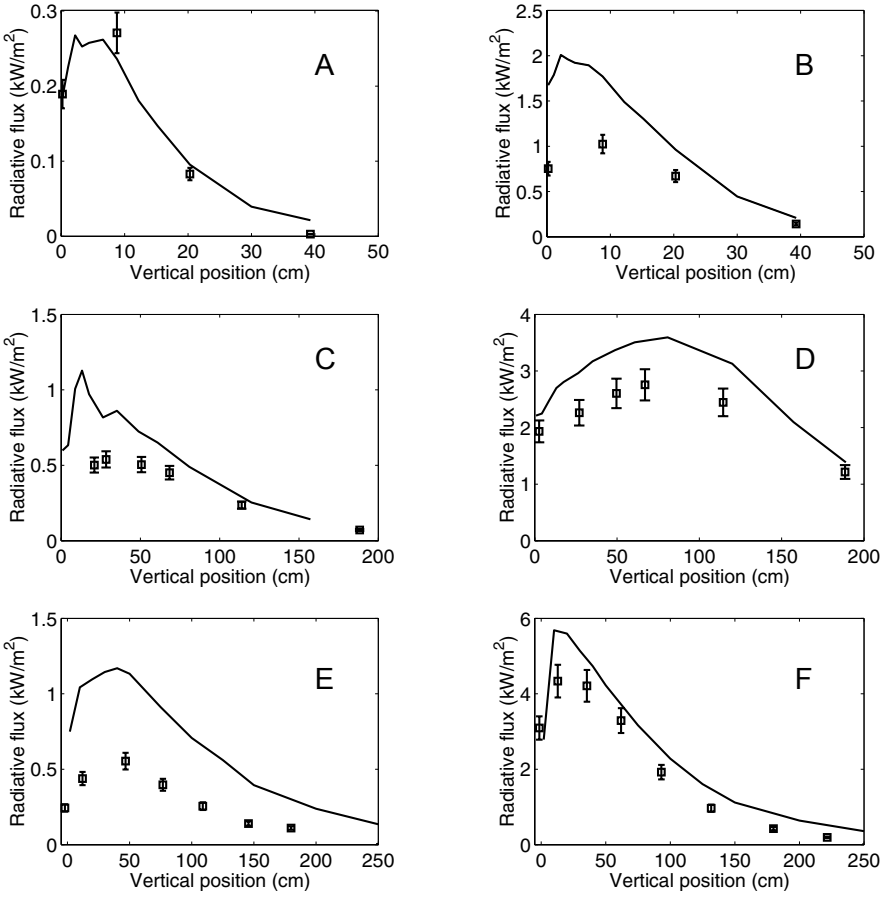


*Figure 15. Comparison of the measured (squares) and predicted (lines) vertical heat flux distributions.*

where $d_m$ is the median droplet diameter, and $\gamma$ and $\sigma$ are empirical constants equal to about 2.4 and 0.6, respectively. In the experiments, Murrel et al. did not measure the droplet diameters in the vicinity of the nozzles, but 0.7 m below the nozzle, i.e. at the height of the heat flux measurement point. The droplet size boundary condition was therefore determined by iterating the initial $d_m$ until the simulated and measured mean diameters at the measurement location were equal, with a few percent tolerance. The iteration was performed for all nozzle-flow rate combinations. The droplet speeds on the inflow boundaries were set equal to the measured vertical velocity component 0.7 m below the nozzle.

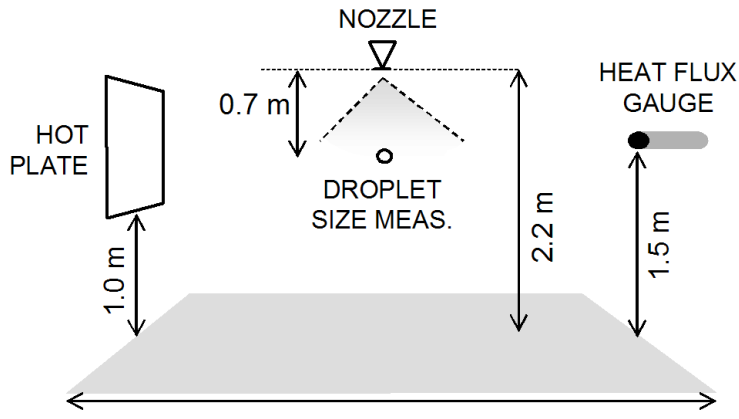


*Figure 16. Schematics of the large-scale attenuation test.*

In the computations, 10 cm grid cells, 1000 control angles, only one spectral band (grey assumption) and no gas phase absorption were used. The measured and predicted attenuation results are compared in Figure 17. Since a good general agreement was found for all three nozzles, and the results of the individual nozzles are well distinct in the flow-rate vs. attenuation space, we can assume that the model can properly take into account both the effect of the water load and the effect of the droplet size distribution. Only the mid-range flow rates of nozzle B and the highest flow rates of nozzle D show sizable discrepancies. These discrepancies are probably caused by a combination of measurement errors and model inaccuracy. The droplet size measurements, in particular, are difficult to conduct in large-scale sprays. The various challenges of spray measurements have been presented by Husted [130]. Some uncertainty is also related to the inverse determination of droplet size boundary conditions for the simulations.

The second validation test for spray-radiation interaction is the experiments of Dembele et al. [131]. They measured the attenuation of a collimated radiation beam passing through a water spray using a Fourier infrared spectrometer. The radiation source was a tungsten filament inside a silica tube. Its emission spectrum was close to that of a blackbody at 1300°C. The spray was produced with one, two or three hydraulic nozzles arranged in a row, and the measurements were made 20 cm below the nozzles at different flow rates. The schematics of the scenario are shown in Figure 18.

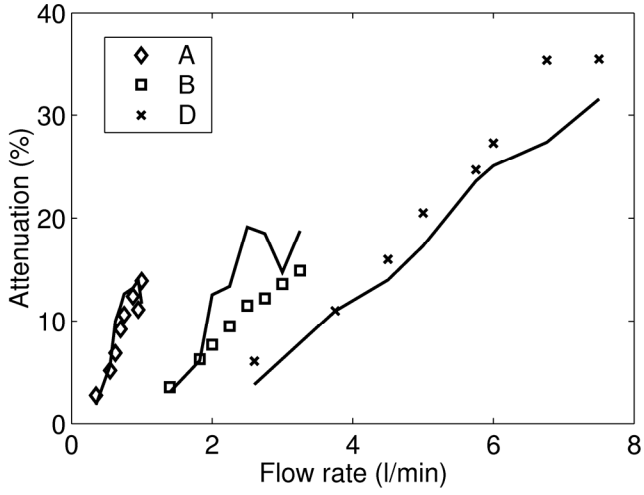


*Figure 17. Results of the large scale attenuation.*

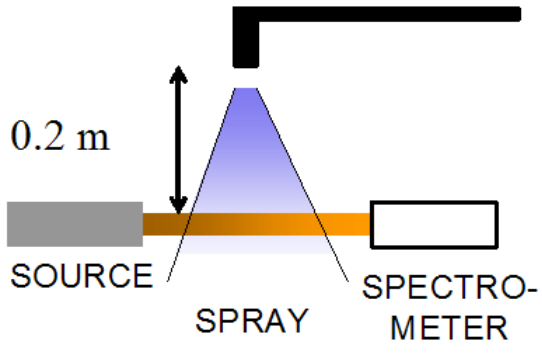


*Figure 18. Schematics of the small-scale attenuation test.*

The simulations were performed at four different flow rates. The droplet size boundary conditions were determined using a procedure similar to the large-scale scenario. The velocity of the droplets at the inflow boundary was found from a simple geometrically based relationship between the flow velocity and distance. Modelling a collimated radiation beam is difficult with FVM due to the symmetric discretization of the unit sphere into solid angles. To alleviate the problem, the radiation source in this exercise was modelled simply as a 4 cm by 4 cm diffuse surface. Despite the strong approximation of the radiation source, the comparison with the measurements is valid on the opposite side of the spray

because the air surrounding the water spray was transparent and non-scattering, but not in the other directions. 2.0 cm grid cells, 1000 radiation angles and six radiation bands were used, but the gas phase absorption was neglected. In this scenario, the independence of the spatial and angular resolutions was very difficult to achieve. For a single-nozzle flow at 0.14 L/min, reducing the cell size from 2.0 cm to 1.0 cm increased the attenuation from 8.3% to 11.4%, with 10.0% being the experimental value. The convergence in angular resolution was difficult to achieve because the radiation source was very small compared to the domain size, and because the ray effect is difficult to avoid in direction of grid axis.

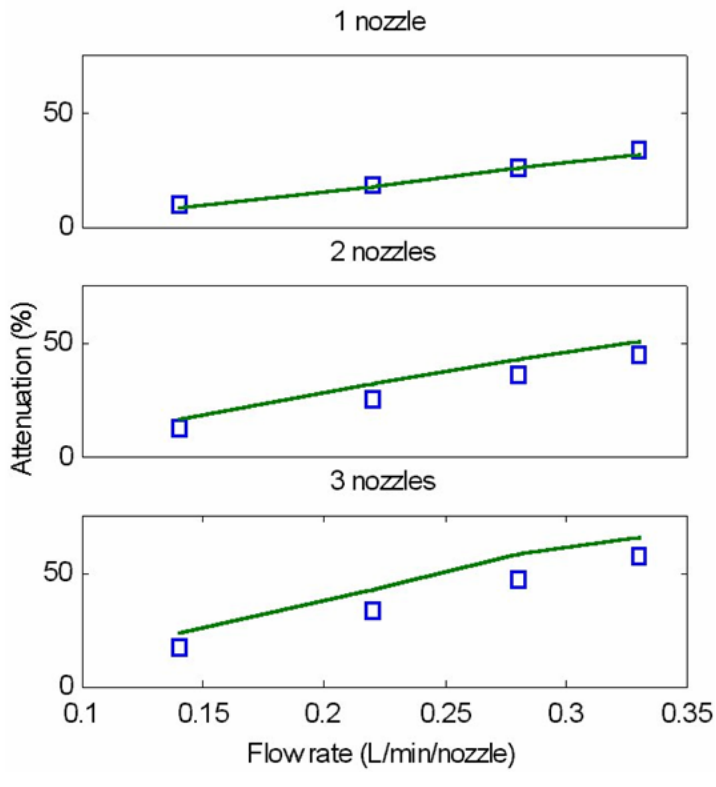


*Figure 19. Comparison of measured (squares) and predicted (lines) attenuation in small-scale tests.*

The measured and simulated attenuation results are compared in Figure 19. In the case of only one nozzle, the agreement is very good, taking into account the unavoidable dependence on the grid and angular resolutions. The root mean-square error between the predicted and measured attenuations is only 1.3%.

When more nozzles are put between the source and the measurement point, the attenuation is clearly over-predicted. The rms errors for two and three nozzles are 6.4 and 8.8%, respectively. One possible reason for the over prediction is the droplet coalescence, which is not taken into account by the model. Coalescence happens as a result of the hydrodynamic interaction between adjacent sprays [131]. This explanation is supported by the finding that while the predicted attenuations with two and three nozzles increase roughly by factors two and three from the values corresponding to the one nozzle, the experimental results increase only by factors of 1.3 and 1.8.

In Paper V, the computed droplet size distributions in different parts of the spray were compared, demonstrating that both the mean diameters and the shapes of the droplet size distributions may vary significantly in different parts of the spray. The same phenomena for hollow cone water mist sprays has been observed experimentally by Husted [130]. During the computation of the mean radiative properties for the spray in this work, the shape of the distribution is fixed to the presumed size probability density function, and only the droplet mean is allowed to vary according to the statistics predicted by the Lagrangian transport model. The importance of this approximation to the radiation solutions is not known, and should be studied in the future.

# 8. Discussion

The applicability of a numerical solver for the intended use depends on the accuracy, computational efficiency and reliability. In this context, the computational efficiency must be measured as a balance between accuracy and computational cost in relation to the rest of the computational framework. Since the intended use of FDS is mainly fire engineering and fire risk analysis, the radiation solver must be efficient and in concordance with the rest of the code to allow *sufficiently* accurate predictions with limited resources. According to Howard Baum, NIST Research Fellow, the CPU consumption of a given numerical routine ought to be commensurate with the particular phenomenon addressed [132]. In a simulation of a typical enclosure fire, where the fraction of heat transfer by radiation is around 30%, the FVM radiation solver consumes less than 30% of the total CPU time. At the same time, the accuracy of the radiation solution is expected to be of the same order with the other phenomena. More accuracy can be achieved by the increased angular, spatial, spectral and temporal resolutions, but at the expense of the increased CPU time. Other requirements, caused by the wide range of uses, are versatility, ease of use and ease of extension.

The presented verification cases demonstrated that in the case of three-dimensional radiation fields, FDS predictions converged towards the exact solutions when *both* spatial *and* angular resolutions were sufficient. In practical simulations, the spatial resolution is usually determined by the flow solution, and the default angular resolution of 104 directions seems to be an appropriate choice. It is important though that the code users are aware of the ray effect and the resulting errors when dealing with heat transfer dominated by far field radiation. The ray effect probably has more importance in code validation, where local radiative fluxes are compared against experiments, than in practical applications.

The validation of the flame radiation computation was performed using diffusion flames ranging from 10 to 100 cm. With few exceptions, the predictions were within 25 % of the measured radiative heat fluxes. Further developments in combustion and radiation source modelling are needed to improve the flame heat fluxes. This is especially true for small heat release rates because the problems appear when the combustion region close to the burning surface is not adequately resolved.

The accuracy of predicting the radiation attenuation by water spray was even better than in the case of flame heat fluxes, demonstrating that the physics of radiation-spray interaction are included with sufficient detail. Aspects of droplet breakup and coalescence should be considered to account for more complicated and dense sprays. Ultimately, the inclusion of secondary droplet breakup could reduce the sensitivity to the droplet size boundary conditions by allowing automatic adjustment of the droplet size according to the flow conditions. However, as pointed out by Madsen [112], the exact mechanisms behind the droplet breakup are still not completely understood. Prediction of the initial atomization processes from the first principles would require very detailed models of the nozzles and relatively complicated models of the two-phase flows, and seems to be beyond the current capabilities of fire simulation.

Due to the challenges of describing the experimental conditions, the angular resolutions and computational costs of the validation simulations were higher than the normal practice in applications. To evaluate the accuracy and cost in situations corresponding to the typical use of the code, a validation study involving real flames and water sprays from sprinklers or water mist nozzles would be needed.

# 9. Concluding remarks

## 9.1 Summary

The objective of this thesis has been to summarize the work of the author in the development of the computational tools for fire risk analysis and fire safety engineering. The work reported in this thesis focused on two particular topics: The first topic was the application of Monte Carlo simulation in the field of fire risk analysis and the development of the necessary tools for performing these simulations using a range of different fire models. The second topic was the development of a numerical solver for the transport of thermal radiation within Fire Dynamics Simulator code. The two topics are linked by the numerous applications of FDS as a deterministic model in fire risk analysis. The efficient and robust radiation solver, developed in the second part of the thesis, will thus benefit the application of the technique developed in the first part.

## 9.2 Development of probabilistic fire simulation

In fire risk analysis, the probabilities of fire consequences are computed using deterministic models for fire phenomena, taking into account the statistical variation or uncertainty of the initial and boundary conditions. The development of the computational resources has allowed the use of Monte Carlo simulation, the most general approach where the space of possible answers is covered in a statistically satisfactory manner. However, the convergence of the Monte Carlo simulation must be accelerated when computationally expensive tools such as CFD are used. The TMMC technique, developed in this work, allows the use of relatively simple and fast models in the collection of the main body of the statistical data, while retaining the physical accuracy by running a small set of simulations with more accurate but slower model and introducing a multi-dimensional scaling function to provide a correction to the main data. The performance of TMMC was validated using simple room fire scenarios, and the use of the FDS code as a deterministic tool of the Monte Carlo simulation was demonstrated.

## 9.3 Weaknesses of TMMC technique and suggestions for future work

The principal weakness of TMMC is a limited knowledge of its theoretical basis. Although it has been seen heuristically to yield good results, and the mechanism is understood, the evidence is not yet sufficient. In the examples presented, the method works well, but there is no general guarantee that the process converges towards the true solution if the fast and slow models differ considerably.

For economy, the accuracy and efficiency of the TMMC technique could be improved by a better numerical treatment of the scaling process. Possible reduction of the number of scaling points should be studied in the future because in some applications, the derivation of the scaling function may form the majority of the computational cost. As demonstrated in the second validation test, all the available a priori information on the relative importance of the random variables should be used to concentrate more scaling points to the most important variables. The application of adaptive sampling techniques to the scaling point placement should be studied in order to reduce the cost in the situations where a priori information is not valid. An example of such a situation is when the inaccuracy of the simple model (Model A) would lead to wrong conclusions on the relative importance of the random variables. Further improvement of the accuracy could be achieved by interpolating the scaling functions between the scaling points to ensure a smoother transition from one scaling region to another.

## 9.4 Development of radiation solver for Fire Dynamics Simulator

During the last few years, CFD fire simulation has become a routine part of fire engineering. This is especially true in the field of design work, where the introduction of a performance-based design concept has created a market for simulation tools that are reliable and accurate enough for the given purpose, and that are fast and relatively easy to use. After its release in 2000, FDS has become the most widely used fire simulation tool in the world. From the code reliability viewpoint, the high number of active users is an advantage, since the wide range of different applications inevitably reveals the errors in the code. The width of

the range also means that some of the applications push the limits of the code in terms of both applicability and validity. On the other hand, the widespread use of CFD may have lured the audience into a sense of complacency with its visually appealing presentation. As a result, CFD may be used or requested when more simple techniques would suffice.

In this work, an FVM-based radiation solver was implemented in FDS. The solver can be used to compute the transport of thermal radiation in a participating medium consisting of combustion gases, soot and water droplets. The goal of the solver implementation was to find a balance between accuracy and computational cost in engineering applications. In the presented verification and validation examples, the accuracy of the predictions was found sufficient for engineering purposes. The highest errors were found in predictions of heat fluxes from weak flames. Computational efficiency was achieved by making three major approximations. First, the use of rectilinear grids in spatial discretization, which is consistent with the rest of the code, increases the computational efficiency by allowing the use of an explicit marching scheme as a method for transport solution and reduces the memory requirement because the geometrical coefficients of the discretized RTE are constants over the whole domain. As a second approximation, the time accuracy of the radiation solution was relaxed by assuming that the numerical time step of the hydrodynamic solver, given by the CFL-condition, is much smaller than the time scale of the global heat transfer processes. The third approximation was the spectral averaging over wide wavelength regions. Additional efficiency was achieved by the extensive use of lookup tables and application of first order accurate scheme for intensities. The high numerical diffusion caused by the first order accuracy was not found to adversely affect the model accuracy.

An important enhancement of the basic radiation solver was the introduction of radiation-spray interactions. Despite the complexity of the physical phenomena, the computational cost of the radiation solution remained in balance with the physical importance. The major approximations were the assumed global similarity of the droplet size distributions and the approximation of scattering phase functions by a sum of isotropic and forward components. Speed of the solution was again achieved by computing the spray radiative properties in advance and storing in lookup tables.

## 9.5 Weaknesses of the radiation solver and suggestions for future work

Some of the model approximations are deeply embedded and improvements in the corresponding code capabilities would be difficult to carry out. The influences of other approximations, however, are more easily controlled by adjusting the model parameters. For example, the extension of the FDS capability with respect to the rectilinearity of the grid would require a complete revision of the radiation solver, whereas an accurate simulation of turbulence-radiation interactions could be implemented simply by adjusting the time interval of the radiation updates. Naturally, higher computational costs should then be expected.

Topics of future work include the generalization of the spectral band structure to allow the use of arbitrary species in the computation of absorption coefficients, generalization of the dispersed phase radiative properties beyond those of water, and allowing the suspensions of other types of particles than liquid droplets. For example, soot is known to both absorb and scatter radiation, but currently only the absorption is taken into account via RadCal. The water spray validation examples demonstrated that the shapes of the droplet size distributions may vary significantly in different parts of the spray. The effect of the global size distribution similarity approximation is currently not known and should be studied in the future by comparing against simulations where the local droplet size distributions are rigorously taken into account in the computation of spray radiative properties. Inclusion of secondary droplet breakup and coalescence processes may be necessary in order to reduce the sensitivity to the droplet size boundary conditions. In addition, a validation of the model using realistic sources of radiation and relevant water spray types should be performed.

In large scale fire simulations, the increase in spatial resolution that would be necessary for a detailed solution of the flame temperature distribution will not be possible for a long time. The modelling of the radiative source term is therefore needed in order to reduce the sensitivity on the unavoidable temperature errors. The current model is based on the assumption of local radiative fraction of heat release, and may be insufficient in fires where the flame optical properties change considerably. An example of such a situation is the transition from a well-ventilated to an under-ventilated enclosure fire. Possible means of

modelling could use the ideas of flamelets, adapted to the practical restrictions of large-scale simulations. A special problem is flame spread on a material, where the process essentially becomes two-dimensional. Application of submodels, similar to the boundary layer theory of Prandtl, might be feasible [133]. Interfacing them to LES codes and addressing the whole problem of wall functions is an issue still to be studied. One practical tool for studying the existence and shape of the flame spread wall functions could be the direct numerical simulation (DNS) of the near wall phenomena. In DNS, all the turbulent length scales are resolved by using very fine spatial resolution and sufficiently accurate numerical schemes. A two-dimensional approximation of DNS may already be possible using the existing tools. DNS can also serve as a detailed tool for experimental design.

# References


1. Molak, V. (ed.) Fundamentals of Risk Analysis and Risk Management. Boca Raton: Lewis Publishers, 1997. 472 p.

2. The Reactor Safety Study – An Assessment of Accident Risks in U.S. Commercial Nuclear Power Plants. Washington, D.C.: U.S. Nuclear Regulatory Commission (USNRC), 1975. WASH-1400 (NUREG-75/014).

3. Severe Accident Risks: An Assessment for Five U.S. Nuclear Power Plants. Washington, D.C.: U.S. Nuclear Regulatory Commission (USNRC), 1991. NUREG-1150.

4. Kaiser, G.D. Overall assessment. In: Green, A.E. (ed.). High Risk Safety Technology. Chichester: Wiley, 1982. Pp. 101–110.

5. PRA Procedures Guide – A Guide to the Performance of Probabilistic Risk Assessment for Nuclear Power Plants. Washington, D.C.: U.S. Nuclear Regulatory Commission (USNRC), 1983. NUREG/CR2300.

6. Keski-Rahkonen, O. Fire safety research (FISRE): FISRE summary report. In: Kyrki-Rajamäki, R. & Puska, E.-K. (eds.). FINNUS The Finnish Research Programme on Nuclear Power Plant Safety 1999–2002. Final Report. Espoo: VTT Processes, 2002. VTT Research Notes 2164. Pp. 197–204.

7. Keski-Rahkonen, O., Mangs, J., Hostikka, S. & Korhonen, T. POTFIS summary report. In: Räty, H. & Puska, E.K. (ed.). SAFIR. The Finnish Research Programme on Nuclear Power Plant Safety 2003–2006. Final Report. Espoo: VTT, 2006. VTT Research Notes 2363. Pp. 335–342.

8. Keski-Rahkonen, O., Mangs, J., Hostikka, S. & Korhonen, T. Quantitative assessment of potential fire spread in nuclear power plant scenarios. In: Post-Conference Seminar III of the 18th International Conference on Structural Mechanics in Reactor Technology (SMIRT 18). 2005. 9th International Seminar on Fire Safety in Nuclear Power Plants and Installations. August 22–24, 2005, Vienna, Austria. CD-ROM.

9. Keski-Rahkonen, O., Mangs, J., Hostikka, S. & Korhonen, T. Quantitative application of Monte Carlo simulation in Fire-PSA. Kerntechnik, 2007. Vol. 72, No. 3, pp. 149–155.

10. Karlsson, B. & Tomasson, B. Repeatability Tests of a Fire Risk Index Method for Multi-Storey Apartment Buildings. In: Gottuk, D.T. & Lattimer, B.Y. (eds.). Proceedings of Eighth International Symposium on Fire Safety Science. Beijing, China, September 18–23, 2005. International Association for Fire Safety Science, 2005. Pp. 901–912.

11. Williamson, R.B. Coupling Deterministic and Stochastic Modeling to Unwanted Fire. Fire Safety Journal, 1981.Vol. 3, pp. 243–259.

12. Ling, W. C. T. & Williamson, R. B. Use of Probabilistic Networks for Analysis of Smoke Spread and the Egress of People in Buildings. In: Grant, C.E. & Pagni, P.J. (Eds.). Proceedings of 1st International Symposium. Fire Safety Science. October 7–11, 1985, Gaithersburg, MD. International Association for Fire Safety Science. Hemisphere Publishing Corp., NY, 1986. Pp. 953–962.

13. Korhonen, T. Hietaniemi, J., Baroudi, D. & Kokkala, M. Time-dependent event-tree method for fire risk analysis: tentative results. In: Evans, D.D. (ed.). Proceedings of the Seventh International Symposium on Fire Safety Science. Worcester, MA, 16–21 June 2003. International Association for Fire Safety Science, 2003. Pp. 321–332.

14. Fontana, M. & Maag, T. Fire Risk Assessment Based on Bayesian Networks. In: Almand, K., Attlan, J.M., D'Hoop, J.M. & Gordon, J. (eds.) Proceedings of 5th International Conference on Performance-Based Codes and Fire Safety Design Methods. October 6–8, 2004, Luxembourg. 2004. Pp. 238–249.

15. Frantzich, H. Risk Analysis and Fire Safety Engineering. Fire Safety Journal, 1998. Vol. 31, No. 4, pp. 313–329.

16. Korhonen, T., Hostikka, S. & Keski-Rahkonen, O. A proposal for the goals and new techniques of modelling pedestrian evacuation in fires. In: Gottuk, D. & Lattimer, B. (eds.). Proceedings of the Eight International Symposium on Fire Safety Science. Beijing, China, 18–23 Sept. 2005. International Association for Fire Safety Science, 2005. Pp. 557–569.

17. Helton, J. C. Treatment of Uncertainty in Performance Assessments for Complex Systems. Risk Analysis, 1994. Vol. 14, No. 4, pp. 483–511.

18. Tillander, K. & Keski-Rahkonen, O. The Ignition Frequency of Structural Fires in Finland 1996–99. In: Evans, D.D. (ed.). Proceedings of the Seventh International Symposium on Fire Safety Science. Worcester, MA, 16–21 June 2003. International Association for Fire Safety Science, 2003. Pp. 1051–1062.

19. Tillander, K. Utilisation of statistics to assess fire risks in buildings. Espoo: VTT Building and Transport, 2004. VTT Publications 537. 224 p. + app. 37 p.

20. Sekizawa, A. Fire Risk Analysis: Its Validity and Potential for Application in Fire Safety. In: Gottuk, D.T. & Lattimer, B.Y. (eds.). Proceedings of Eighth International Symposium on Fire Safety Science. Beijing, China, September 18–23, 2005. International Association for Fire Safety Science, 2005. Pp. 82–100.

21. Vose, D. Monte Carlo Risk Analysis Modeling. In: Molak, V. (ed.). Fundamentals of Risk Analysis and Risk Management. Boca Raton: Lewis Publishers, 1997. 472 p.

22. Metropolis, N. & Ulam, S. The Monte Carlo Method. Journal of the American Statistical Association, 1949. Vol. 44, No. 247, pp. 335–341.

23. Vose, D. Quantitative risk analysis: a guide to Monte Carlo simulation modelling. Chichester, England: Wiley, 1996. 328 p.

24. Hofer, E., Jahn, H. & Krzykacz, B. Uncertainty and sensitivity analysis of an oil and cable fire simulation with the code CRDLOC. In: Apostolakis, G. (ed.) Probabilistic Safety Assessment and Management, Elsevier Science Publishing Co., 1991.

25. Krzykacz, B., Hofer, E. & Kloos, M. A software system for probabilistic uncertainty and sensitivity analysis of results from computer models. In: Proceedings of PSAM II. San Diego, CA, USA, 20–25 March 1994.

26. Hostikka, S., Keski-Rahkonen, O. & Korhonen, T. Probabilistic Fire Simulator. Theory and User's Manual for Version 1.2, Espoo: VTT Building and Transport, 2003. VTT Publications 503, 72 p. + App. 1 p.

27. McKay, M.D., Beckman, R.J. & Conover, W.J. A comparison of three methods for selecting values of input variables in the analysis of output from a computer code. Technometrics, 1979. Vol. 21, No. 2, pp. 239–245.

28. Iman, R.L. & Helton, J.C. Investigation of Uncertainty and Sensitivity Analysis Techniques for Computer Models. Risk Analysis, 1988. Vol. 8, No. 1, pp. 71–90.

29. Magnussion, S.E. Risk Assessment. International Association for Fire Safety Science. In: Hasemi, Y. (ed.) Proceedings of Fifth (5th) International Symposium on Fire Safety Science. March 3–7, 1997, Melbourne, Australia. Boston, MA: International Association for Fire Safety Science, 1997. Pp. 41–58.

30. Hofer, E., Kloos, M., Krzykacz, B., Peschke, J. & Sonnenkalb, M. Methodenentwicklung zur simulativen Behandlung der Stochastik in probabilistischen Sicherheitsanalysen der Stufe 2. Garching: GRSA-2997, Gesellschaft für Anlagen- und Reaktorsicherheit, 2001.

31. Hofer, E, Kloos, M., Krzykacz-Hausmann, B. Peschke, J. & Woltereck, M. An approximate epistemic uncertainty analysis approach in the presence of epistemic and aleatory uncertainties, Reliability Engineering and System Safety, 2002. Vol. 77, pp. 229–238.

32. Eschenroeder, A.Q. & Faeder, E.J. Monte Carlo Analysis of Health Risks From PCB-Contaminated Mineral Oil Transformer Fires. Risk Analysis, 1988. Vol. 8, No. 2, pp. 291–298.

33. Zhao, L. Methodology of Calculating the Risk to People in Building Fires. In: Shields, J. (ed.). Proceedings of 1st International Symposium on Human Behavior in Fire. August 31 – September 2, 1998, Belfast, Northern Ireland. Northern Ireland: University of Ulster, 1998. Pp. 401–410.

34. Fraser-Mitchell, J. Risk Assessment of Factors Related to Fire Protection in Dwellings. In: Hasemi, Y. (ed.) Proceedings of Fifth (5th) International Symposium on Fire Safety Science. March 3–7, 1997, Melbourne,

Australia. Boston, MA: International Association for Fire Safety Science, 1997. Pp. 631–642.

35. Magnusson, S.E., Frantzich, H. & Harada, K. Fire Safety Design Based on Calculations: Uncertainty Analysis and Safety Verification. Fire Safety Journal, 1996. Vol. 27, pp. 305–334.

36. Fraser-Mitchell, J.N. Modelling Human Behavior Within the Fire Risk Assessment Tool "CRISP". In: Shields, J. (ed.). Proceedings of 1st International Symposium on Human Behavior in Fire. August 31 – September 2, 1998, Belfast, Northern Ireland. Northern Ireland: University of Ulster, 1998. Pp. 447–457.

37. Zhao, L. & Beck, V. Definition of Scenarios for the CESARE-RISK Model. In: Hasemi, Y. (ed.) Proceedings of Fifth (5th) International Symposium on Fire Safety Science. March 3–7, 1997, Melbourne, Australia. Boston, MA: International Association for Fire Safety Science, 1997. Pp. 655–666.

38. Phillips, W.G.B. Simulation Models for Fire Risk Assessment. Fire Safety Journal, 1994. Vol. 23, No. 2, pp. 159–169.

39. Hasofer, A.M. & Qu, J. Response Surface Modelling of Monte Carlo Fire Data. Fire Safety Journal, 2002. Vol. 37, No. 8, pp. 772–784.

40. Notarianni, K.A. Role of Uncertainty in Improving Fire Protection Regulation. Pittsburgh, PA: Carnegie-Mellon Univ. 2000. Thesis, 269 p.

41. Hamilton, S.R. & Deierlein, G.G. Probabilistic Methodology for Performance-Based Fire Engineering. In: Almand, K., Attlan, J.M., D'Hoop, J.M. & Gordon, J. (eds.) Proceedings of 5th International Conference on Performance-Based Codes and Fire Safety Design Methods. October 6–8, 2004, Luxembourg. 2004. Pp. 327–341.

42. Kirby, B.R., Newman, G.M., Butterworth, N., Pagan, J. & English, C. Development of a Performance Based Approach to Specifying Fire Resistance for Regulatory Purposes. In: Almand, K., Attlan, J.M., D'Hoop, J.M. & Gordon, J. (eds.) Proceedings of 5th International Conference on Performance-Based Codes and Fire Safety Design Methods. October 6–8, 2004, Luxembourg. 2004. Pp. 183–194.

43. Li, Y. & Spearpoint, M. Cost-Benefit Analysis of Sprinklers for Property Protection in New Zealand Parking Buildings. Journal of Applied Fire Science, 2003–2004. Vol. 12, No. 3, pp. 223–243.

44. Yuen, W.W. & Chow, W.K. Monte Carlo Approach for the Layout Design of Thermal Fire Detection System. Fire Technology, 2005. Vol. 41, No. 2, pp. 93–104.

45. Madras, N. Lectures on Monte Carlo methods. Providence, RI: American Mathematical Society, 2002. 103 p.

46. Landau, D.P. & Binder, K.A guide to Monte Carlo simulations in statistical physics. Cambridge University Press, 2005. 2nd ed. 432 p.

47. Milton, J.S. & Arnold, J.C. Introduction to probability and statistics: principles and applications for engineering and the computing sciences. New York, NY: McGraw-Hill, 1990. 2nd ed. 700 p.

48. Stein, M.L. Large sample properties of simulations using latin hypercube sampling. Technometrics, 1987. Vol. 29, No. 2, pp. 143–151.

49. Hofer, E. Sensitivity analysis in the context of uncertainty analysis for computationally intensive models. Computer Physics Communications, 1999. Vol. 117, pp. 21–34.

50. Pebesma, E.J. & Heuvelink, G.B.M. Latin hypercube sampling of multigaussian random fields. Technometrics, 1999. Vol. 41, No. 4, pp. 303–312.

51. Jones, W.W., Forney, G.P., Peacock, R.D. & Reneke, P.A. Technical Reference for CFAST: An Engineering Tool for Estimating Fire and Smoke Transport. Gaithersburg, MD: National Institute of Standards and Technology, 2000. NIST TN 1431. 190 p.

52. Cadorin, J.-F. & Franssen, J.-M. A tool to design steel elements submitted to compartment fires-OZone V2. Part 1: Pre-and post-flashover compartment fire model. Fire Safety Science, 2003. Vol. 38, No. 5, pp. 395–427.

53. Cadorin, J.-F., Pintea, D., Dotreppe, J.-C. & Franssen, J.-M. A tool to design steel elements submitted to compartment fires-OZone V2. Part 2: Methodology and application. Fire Safety Science, 2003. Vol. 38, No. 5, pp. 429–451.

54. Vaari, J. A transient one-zone computer model for total flooding water mist fire suppression in ventilated enclosures. Fire Safety Journal, 2002. Vol. 37, No. 3, pp. 229–257.

55. Drysdale, D. An Introduction to Fire Dynamics. Chichester: Wiley-Interscience, 1999. Second Edition, 140 p.

56. Hostikka, S. & Keski-Rahkonen, O. Advanced probabilistic simulation of NPP fires. Proceedings of the 18th International Conference on Structural Mechanics in Reactor Technology. SMIRT 18. Beijing, China, August 7–12, 2005. Beijing: Atomic Energy Press, 2005. Pp. 3984–3996.

57. Raithby, G.D. & Chui, E.H. A Finite-Volume Method for Predicting Radiant Heat Transfer in Enclosures with Participating Media. Journal of Heat Transfer, 1990. Vol. 112, No. 2, pp. 415–423.

58. Cox, G. & Kumar, S. Modelling Enclosure Fires Using CFD. In: SFPE Handbook of Fire Protection Engineering. Quincy, MA: Society of Fire Protection Engineers, 2002. 3rd Edition. Pp. 3-194–3-218.

59. Patankar, S.V. & Spalding, D.B.A Calculation Procedure for Heat, Mass and Momentum Transfer in Three-dimensional Parabolic Flows. International Journal for Heat and Mass Transfer, 1972. Vol. 15, pp. 1787–1806.

60. Magnussen B. & Hjertager G.H. On mathematical modelling of turbulent combustion with special emphasis on soot formation and combustion. In: Proceedings of 16th International Symposium on Combustion. The Combustion Institute, 1976. Pp. 719–729.

61. McGrattan, K.B., Hostikka, S., Floyd, J.E., Baum, H. & Rehm, R. Fire Dynamics Simulator (Version 5): Technical Reference Guide. Gaithersburg, MD: National Institute of Standards and Technology, October 2007. NIST Special Publication 1018-5.

62. McGrattan, K.B., Klein, B., Hostikka, S. & Floyd, J.E. Fire Dynamics Simulator (Version 5): User's Guide. Gaithersburg, MD: National Institute of Standards and Technology, October 2007. NIST Special Publication 1019-5.

63. Olenick, S. & Carpenter, D. An Updated International Survey of Computer Models for Fire and Smoke. Journal of Fire Protection Engineering, 2003. Vol. 13, pp. 87–110.

64. Ferziger, J.H. & Perić, M. Computational Methods for Fluid Dynamics. Heidelberg: Springer, 1997. Corrected 2nd printing. 364 p.

65. Courant, R. Friedrichs, K.O. & Lewy, H. Über die partiellen Differential-gleichungen der mathematischen Physik. Mathematische Annalen 100, 1928. Pp. 32–74.

66. Courant, R., Friedrichs, K. & Lewy, H. On the partial difference equations of mathematical physics. IBM Journal, 1967, pp. 215–234. English translation of the 1928 German original paper.

67. Baum, H.R. & Rehm, R.G. Calculations of Three Dimensional Buoyant Plumes in Enclosures. Combustion Science and Technology, 1984. Vol. 40, pp. 55–77.

68. Holen, J., Brostrom, M. & Magnussen, B.F. Finite Difference Calculation of Pool Fires. In: Proceedings of the 23rd Symposium (International) on Combustion, Combustion Institute, 1990. Pp. 1677–1683.

69. Taylor, S., Petridis, M., Knight, B., Ewer, J., Galea, E.R & Patel, M. SMARTFIRE: an integrated computational fluid dynamics code and expert system for fire field modelling. In: Hasemi, Y. (ed.) Proceedings of Fifth (5th) International Symposium on Fire Safety Science. March 3–7, 1997, Melbourne, Australia. Boston, MA: International Association for Fire Safety Science, 1997. Pp. 1285–1296.

70. Welch, S. & Rubini, P. Three-Dimensional Simulation of a Fire-Resistance Furnace. In: Hasemi, Y. (ed.) Proceedings of Fifth (5th) International Symposium on Fire Safety Science. March 3–7, 1997, Melbourne, Australia. Boston, MA: International Association for Fire Safety Science, 1997. Pp. 1009–1020.

71. Suard, S., Audouin, L., Babik, F., Rigollet, L. & Latche, J.C. Verification and Validation of the ISIS CFD Code for Fire Simulation. Workshop on Assessment of Calculation Methods in Fire Safety Engineering, San antonio, TX, USA, 10 April 2006. ISO/TC 92/SC4. 28 p.

72. Greiner, M. & Suo-Anttila, A. Radiation Heat Transfer and Reaction Chemistry Models for Risk Assessment Compatible Fire Simulations. Journal of Fire Protection Engineering, 2006. Vol. 16, No. 2, pp. 79–104.

73. Yan, Z. Large Eddy Simulation of Soot Formation in a Turbulent Diffusion Flame. In: Gottuk, D.T. & Lattimer, B.Y. (eds.). Proceedings of Eighth International Symposium on Fire Safety Science. Beijing, China, September 18–23, 2005. International Association for Fire Safety Science, 2005. Poster abstract.

74. Cheung, A.L.K., Cheung, S.C.P., Yeoh, G.H. & Yuen, R.K.K. Investigation of Pulsating Behaviour of Buoyant Fires by Using Large Eddy Simulation (LES) Approach with Soot and Radiation. In: Gottuk, D.T. & Lattimer, B.Y. (eds.). Proceedings of Eighth International Symposium on Fire Safety Science. Beijing, China, September 18–23, 2005. International Association for Fire Safety Science, 2005. Poster abstract.

75. Kumar, S. Mathematical modelling of Natural Convection in Fire – A State of the Art Review of the Field Modelling of Variable Density Turbulent Flow. Fire and Materials, 1983. Vol. 7, pp. 1–24.

76. Liu, F. & Wen, J.X. The effect of different turbulence models on the CFD simulation of buoyant diffusion flames. Fire Safety Journal, 2002. Vol. 37, No. 2, pp. 125–151.

77. McGrattan, K.B., Rehm, R.G. & Baum, H.R. Fire-Driven Flows in Enclosures. Journal of Computational Physics, 1994. Vol. 110, No. 2, pp. 285–291.

78. Rehm, R.G., McGrattan, K.B., Baum, H.R. & Cassel, K.W. Transport by Gravity Currents in Building Fires. In: Fire Safety Science – Proceedings of the Fifth International Symposium. International Association for Fire Safety Science, 1997. Pp. 391–402.

79. Clement, J.M. & Fleischmann, C.M. Experimental Verification of the Fire Dynamics Simulator Hydrodynamic Model. In: Fire Safety Science – Proceedings of the Seventh International Symposium. International Association for Fire Safety Science, 2002. Pp. 839–862

80. Baum, H.R., McGrattan, K.B. & Rehm, R.G. Three Dimensional Simulations of Fire Plume Dynamics. In: Hasemi, Y. (ed.) Proceedings of Fifth (5th) International Symposium on Fire Safety Science. March 3–7, 1997, Melbourne, Australia. Boston, MA: International Association for Fire Safety Science, 1997. Pp. 511–522.

81. Baum, H.R. & McCaffrey, B.J. Fire Induced Flow Field – Theory and Experiment. In: Proceedings of the Second International Symposium on Fire Safety Science. International Association for Fire Safety Science, 1989. Pp. 129–148.

82. McGrattan, K.B., Baum, H.R. & Rehm, R.G. Large Eddy Simulations of Smoke Movement. Fire Safety Journal, 1998. Vol. 30, pp. 161–178.

83. Ma, T.G. & Quintiere, J.G. Numerical simulation of axi-symmetric fire plumes: accuracy and limitations. Fire Safety Journal, 2003. Vol. 38, No. 5, pp. 467–492.

84. Hamins, A., Maranghides, A., McGrattan, K.B., Johnsson, E., Ohlemiller, T., Donnelly, M., Yang, J., Mulholland, G., Prasad, K., Kukuck, S., Anleitner, R. & McAllister, T. Report on Experiments to Validate Fire Dynamic and Thermal-Structural Models for Use in the World Trade Center Investigation. Gaithersburg, MD: National Institute of Standards and Technology, 2004. NIST Special Publication 1000-B.

85. Hamins, A., Maranghides, A., McGrattan, K.B., Ohlemiller, T. & Anletiner, R. Experiments to Validate Models of Fire Growth and Spread for use in the World Trade Center Investigation. Gaithersburg, MD: National Institute of Standards and Technology, 2004. NIST Special Publication 1000-10E.

86. McGrattan, K.B. Verification and Validation of Selected Fire Models for Nuclear Power Plant Applications. Volume 7. Fire Dynamics Simulator (FDS). Gaithersburg, MD: National Institute of Standards and Technology. Washington, DC: Nuclear Regulatory Commission. Palo Alto, CA: Electric Power Research Institute, 2007. NUREG-1824, EPRI 1011999. Volume 7. 205 p.

87. de St. Germain, J.D., McCorquodale, J., Parker, S.G. & Johnson, C.R. Uintah: A Massively Parallel Problem Solving Environment, Ninth IEEE International Symposium on High Performance and Distributed Computing. IEEE, 2000. Pp. 33–41.

88. Pope, S.B. Ten questions concerning the large-eddy simulation of turbulent flows. New Journal of Physics, 2004. Vol. 6, pp. 1–24.

89. Zhang, W., Hamer, A., Klassen, M., Carpenter, D. & Roby, R. Turbulence statistics in a fire room model by large eddy simulation. Fire Safety Journal, 2002. Vol. 37, No. 8, pp. 721–752.

90. Tuovinen, H., Blomqvist, P. & Saric, F. Modelling of hydrogen cyanide formation in room fires. Fire Safety Journal, 2004. Vol. 39, No. 8, pp. 737–755.

91. Yang, R., Weng, W.G., Fan, W.C. & Wang, Y.S. Subgrid scale laminar flamelet model for partially premixed combustion and its application to backdraft simulation. Fire Safety Journal, 2005. Vol. 40, No. 2, pp. 81–98.

92. Kang, Y. & Wen, J. X. Large Eddy Simulation of a Small Pool Fire. Combustion Science and Technology, 2004. Vol. 176, No. 12, pp. 2193–2223.

93. Beyler, C.L. Fire Hazard Calculations for Large, Open Hydrocarbon Fires. In: SFPE Handbook of Fire Protection Engineering. Quincy, MA: Society of Fire Protection Engineers, 2002. 3rd Edition. Pp. 3-268–3-314.

94. Siegel, R. & Howell, J.R. Thermal Radiation Heat Transfer. New York, NY: Hemisphere Publishing Corporation, 1981. 2nd ed. 862 p.

95. Özisik, M.N. Radiative transfer and interactions with conduction and convection. New York, NY: John Wiley & Sons Inc., 1973. 575 p.

96. Lockwood, F.C. & Shah, N.G. A new radiation solution method for incorporation in general combustion prediction procedures. In: Proceedings of the 18th Symposium (International) on Combustion. Pittsburgh, PA: The Combustion Institute, 1981. pp. 1405–1416.

97. Jensen, K.A., Ripoll, J.-F., Wray, A.A., Joseph, D. & El Hafi, M. On various modeling approaches to radiative heat transfer in pool fires. Combustion and Flame, 2007. Vol. 148, No. 4, pp. 263–279.

98. Dembele, S. & Wen, J.X. Evaluation of a fast correlated-k approach for radiation calculations in combustion systems. Numerical Heat Transfer Part B, 2003. Vol. 44, No. 4, pp. 365–385.

99. Dembele, S., Zhang, J. & Wen, J.X. Assessments of Spectral Narrow Band and Weighted-Sum-of-Gray-Gases Models for Computational Fluid Dynamics Simulations of Pool Fires. Numerical Heat Transfer Part B, 2005. Vol. 48, No. 3, pp. 257–276.

100. Zhang, J., Dembele, S., Karwatzki, J. & Wen, J. X. Effect of Radiation Models on CFD Simulations of Upward Flame Spread. In: Gottuk, D.T. & Lattimer, B.Y. (eds.). Proceedings of Eighth International Symposium on Fire Safety Science. Beijing, China, September 18–23, 2005. International Association for Fire Safety Science, 2005. Pp. 421–432.

101. Wiscombe, W. Mie scattering calculations: Advances in technique and fast, vector-speed computer codes. National Center For Atmospheric Research, 1979 (revised 1996). NCAR Technical Note NCAR/TN-140+STR.

102. Bohren, C.F. & Huffman, D.R. Absorption and scattering of light by small particles. New York, NY: John Wiley & Sons, 1983. 530 p.

103. Berour, N., Lacroix, D., Boulet, P. & Jeandel, G. Radiative and conductive heat transfer in a nongrey semitransparent medium. Application to fire protection curtains. Journal of Quantitative Spectroscopy & Radiative Transfer, 2004. Vol. 86, pp. 9–30.

104. Trivic, D.N., O'Brien, T.J. & Amon, C.H. Modeling the radiation of anisotropically scattering media by coupling Mie theory with Finite volume method. International Journal of Heat and Mass Transfer, 2004. Vol. 47, pp. 5765–5780.

105. Collin, A., Boulet, P., Lacroix, D. & Jeandel, G. On radiative transfer in water spray curtains using the discrete ordinates method. Journal of Quantitative Spectroscopy & Radiative Transfer, 2005. Vol. 92, pp. 85–110.

106. Yeoh, G.H., Yuen, R.K.K., Chueng, S.C.P. & Kwok, W.K. On modelling combustion, radiation and soot processes in compartment fires. Building and Environment, 2003. Vol. 38, No. 6, pp. 771–785.

107. Wen, J.X., Huang, L.Y. & Roberts, J. The effect of microscopic and global radiative heat exchange on the field predictions of compartment fires. Fire Safety Journal, 2001. Vol. 36, No. 3, pp. 205–223.

108. Lautenberger, C.W., de Ris, J.L., Dembsey, N.A., Barnett, J.R. & Baum, H.R. A simplified model for soot formation and oxidation in CFD simulation of non premixed hydrocarbon flames. Fire Safety Journal, 2005. Vol. 40, No. 2, pp. 141–176.

109. Prasad, K.R. & Baum, H.R. Coupled Fire Dynamics and Thermal Response of Complex Building Structures. In: Chen, J.H., Colket, M.D., Barlow, R.S. & Yetter, R.A. (eds.). Proceedings of the 30th Symposium (International) on Combustion. July 25–30, 2004, Chicago, IL. Pittsburgh, PA: Combustion Institute, 2005. Vol. 30. Part 2. Pp. 2255–2262.

110. Atreya, A. & Baum, H.R. Model of Opposed-Flow Flame Spread Over Charring Materials. In: Chen, J.H. & Colket, M. D. (eds.). Proceedings of the 29th Symposium (International) on Combustion. July 21–25, 2002, Sapporo, Japan. Pittsburgh, PA: Combustion Institute, 2002. Vol. 29. Part 1. Pp. 227–236.

111. Kim, S.C. & Ryou, H.S. An experimental and numerical study on fire suppression using a water mist in an enclosure. Building and Environment, 2003. Vol. 38, No. 11, pp. 1309–1316.

112. Madsen, J. Computational and Experimental Study of Sprays from the Breakup of Water Sheets. Denmark: Aalborg University Esbjerg, 2006. PhD Thesis. 260 p.

113. Ingram, D.M., Causon, D.M. & Mingham, C.G. Developments in Cartesian cut cell methods. Mathematics and Computers in Simulation, 2003. Vol. 61, pp. 561–572.

114. Gemeny, D.F., Alex, P.E., Kline, A.J. & Hardeman, B. PyroSim: A Dynamic Graphical User Interface for the Fire Dynamics Simulator and Pathfinder: A Companion Egress Model. INTERFLAM 2007. Proceedings of the 11th International Conference. September 3–5, 2007, London, England. Vol. 2, pp. 1417–1422.

115. Heinisuo, M. & Laasonen, M. Product modeling, part of the fire safety concept in the future for metal structures? In: Advanced research workshop on Fire Computer Modeling. Santander, Spain: University of Cantabria. 2007.

116. Dimyadi, J.A.W., Spearpoint, M. & Amor, R. Generating fire dynamics simulator geometrical input using an IFC-based building information model. Electronic Journal of Information Technology in Construction, 2007. Vol. 12, p. 443.

117. Chang, S.L. & Rhee, K.T. Blackbody radiation functions. International Communications in Heat and Mass Transfer, 1984. Vol. 11, pp. 451–455.

118. Grosshandler, W. RadCal: A Narrow Band Model for Radiation Calculations in a Combustion Environment. Gaithersburg, MD: National Institute of Standards and Technology, 1993. NIST Technical Note TN 1402.

119. Kim, S.H. & Huh, K.Y. Assessment of The Finite-Volume Method and The Discrete Ordinate Method for Radiative Heat Transfer In a Three-Dimensional Rectangular Enclosure. Numerical Heat Transfer, Part B, 1999. Vol. 35, pp. 85–112.

120. Murthy, J.Y. & Mathur, S.R. Radiative Heat Transfer in Axisymmetric Geometries Using an Unstructured Finite-Volume Method. Numerical Heat Transfer, Part B, 1998. Vol. 33, pp. 397–416.

121. Raithby, G.D. Discussion of the Finite-Volume Method for Radiation, and its Application Using 3D Unstructured Meshes. Numerical Heat Transfer, Part B, 1999. Vol. 35, pp. 389–405.

122. Chai, J.C., Lee, H.S. & Patankar, S.V. Finite Volume Method for Radiation Heat Transfer. Journal of Thermophysics and Heat Transfer, 1994. Vol. 8, No. 3, pp. 419–425.

123. Ravigururajan, T. & Beltran, M. A Model for Attenuation of Fire Radiation Through Water Droplets. Fire Safety Journal, 1989. Vol. 15, pp. 171–181.

124. Yang, W., Parker, T., Ladouceur, H.D. & Kee, R.J. The Interaction of Thermal Radiation and Water Mist in Fire Suppression. Fire Safety Journal, 2004. Vol. 39, pp. 41–66.

125. Wiscombe, W.J. Improved Mie Scattering Algorithms. Applied Optics, 1980. Vol. 19, No. 9, pp. 1505–1509.

126. Hale, G.M. & Querry, M.R. Optical constants of water in the 200 nm to 200 mum wavelength region. Applied Optics, 1973. Vol. 12, No. 3, pp. 555–563.

127. Zel'dovich, Y.B. & Raizer, Y.P. Physics of shock waves and high-temperature hydrodynamic phenomena. New York, NY: Dover Publications, 2002. Translated from the Russian and then edited by W.D. Hayes and R.F. Probstein.

128. Hamins, A., Klassen, M., Gore, J. & Kashiwagi, T. Estimate of Flame Radiance via a Single Location Measurement in Liquid Pool Fires. Combustion and Flame, 1991. Vol. 86, pp. 223–228.

129. Murrel, J.V., Crowhurst, D. & Rock, P. Experimental study of the thermal radiation attenuation of sprays from selected hydraulic nozzles. In: Proceedings of Halon options technical working conference. The University of New Mexico, Albuquerque, 1995. pp. 369–378.

130. Husted, B.P. Experimental measurements of water mist systems and implications for modelling in CFD. Lund, Sweden: Lund University, 2007. Doctoral Thesis. 124 p. + app.

131. Dembele, S., Wen, J.X. & Sacadura, J.-F. Experimental study of water sprays for the attenuation of fire thermal radiation. Journal of Heat Transfer, 2001. Vol. 123, pp. 534–543.

132. McGrattan, K. B. Fire Modeling: Where Are We? Where Are We Going? In: Gottuk, D.T. & Lattimer, B.Y. (eds.). Proceedings of Eighth International Symposium on Fire Safety Science. Beijing, China, September 18–23, 2005. International Association for Fire Safety Science, 2005. Pp. 53–68.

133. Schlichting, H. Boundary Layer Theory, New York, NY: McGraw-Hill, 1987. 7th reissued ed. 817 p.

# List of related publications


1. Hostikka, S., Baum, H. & McGrattan, K. Large eddy simulation of the cone calorimeter. Proceedings of the 2nd Joint Meeting of the US Sections of the Combustion Institute. Oakland, CA, 25–28 March 2001. Western States Section of the Combustion Institute, 2001.

2. Hostikka, S. & McGrattan, K. Large eddy simulation of wood combustion. INTERFLAM 2001. Proceedings of the 9th International Conference. Edinburgh, GB, 17–19 Sept. 2001. Vol. 1, pp. 755–765.

3. McGrattan, K.B., Floyd, J.E., Forney, G.P., Baum, H.R. & Hostikka, S. Improved radiation and combustion routines for a large eddy simulation fire model. Fire Safety Science. Proceedings of the seventh international symposium. Worcester, MA, 16–21 June 2003. Evans, D.D. (ed.). International Association for Fire Safety Science, 2003, pp. 827–838.

4. Hostikka, S., Keski-Rahkonen, O. & Korhonen, T. Probabilistic Fire Simulator. Theory and User's Manual for Version 1.2, VTT Building and Transport. VTT Publications 503, 2003. 72 p. + app. 1 p.

5. Hietaniemi, J., Hostikka, S. & Korhonen, T. Probabilistic Fire Simulation, Proc. of the 5th Int'l Conference on Performance-Based Codes and Fire Safety Design Methods, Society of Fire Protection Engineers, 2004, pp. 280–291.

6. Hostikka, S. & Keski-Rahkonen, O. Advanced probabilistic simulation of NPP fires. Proceedings of the 18th International Conference on Structural Mechanics in Reactor Technology. SMIRT 18. Beijing, China, August 7–12, 2005. Atomic Energy Press. Beijing (2005), 3984–3996.

7. Keski-Rahkonen, O., Mangs, J., Hostikka, S. & Korhonen, T. Quantitative application of Monte Carlo simulation in Fire-PSA. Kerntechnik, Vol. 72, 3, 2007, pp. 149–155.

8. Heikkinen, J., Hostikka, S., Shemeikka, J. & Kauppinen, T. Prediction of Draught and Surface Temperatures in a Living Room Using CFD. Roomvent 2007, 10th International Conference on Air Distribution in Rooms, Helsinki, Finland, 13–15 June 2007. Finvac ry, 2007.

Series title, number and
report code of publication

VTT Publications 683
VTT-PUBS-683

Author(s)
Hostikka, Simo

Title

# Development of fire simulation models for radiative heat transfer and probabilistic risk assessment

Abstract

In the first part of the work, an engineering tool for probabilistic fire risk assessment has been developed. The tool can be used to perform Monte Carlo simulations of fires and is called Probabilistic Fire Simulator (PFS). In practical applications, advanced simulation techniques based on computational fluid dynamics (CFD) are needed. Due to the high computational cost associated with CFD-based fire simulation, specialized algorithms are needed to allow the use of CFD in Monte Carlo simulation. By the use of the Two-Model Monte Carlo (TMMC) technique, developed in this work, the computational cost can be reduced significantly by combining the results of two different models. The developed technique has been verified and validated by using different combinations of fire models, ranging from analytical formulas to CFD.

In the second part of the work, a numerical solver for thermal radiation has been developed for the Fire Dynamics Simulator code. The solver can be used to compute the transfer of thermal radiation in a mixture of combustion gases, soot and liquid droplets. A new model has been developed for the absorption and scattering by liquid droplets. The radiative properties of droplets are computed using a Mie-theory and averaged locally over the spectrum and presumed droplet size distribution. To simplify the scattering computations, the single-droplet phase function is approximated as a sum of forward and isotropic components. The radiation solver has been verified by comparing the results against analytical solutions and validated by comparisons against experimental data from pool fires and experiments of radiation attenuation by water sprays at two different length scales.

ISBN
978-951-38-7099-7 (soft back ed.)
978-951-38-7100-0 (URL: http://www.vtt.fi/publications/index.jsp)

| Series title and ISSN | Project number |
|---|---|
| VTT Publications<br>1235-0621 (soft back ed.)<br>1455-0849 (URL: http://www.vtt.fi/publications/index.jsp) | |

| Date | Language | Pages |
|---|---|---|
| May 2008 | English, Finnish abstr. | 103 p. + app. 82 p. |

| Keywords | Publisher |
|---|---|
| fire simulation, Monte Carlo simulation, probabilistic risk assessment, thermal radiation, verification, validation | VTT Technical Research Centre of Finland<br>P.O. Box 1000, FI-02044 VTT, Finland<br>Phone internat. +358 20 722 4520<br>Fax +358 20 722 4374 |

Julkaisun sarja, numero ja raporttikoodi

VTT Publications 683
VTT-PUBS-683

Tekijä(t)
Hostikka, Simo

Nimeke

# Tulipalon simuloinnissa käytettävän säteilylämmönsiirto-mallin ja riskianalyysimenetelmän kehittäminen

Tiivistelmä

Paloriskien arvioinnissa on olennaista palon seurausten ja leviämismahdollisuuksien analysointi. Tässä työssä on kehitetty tulipalojen numeerisen simuloinnin malleja ja työkaluja. Työn päätavoitteita ovat olleet palosimuloinnin parhaimpien laskentamallien hyödyntäminen todennäköisyyspohjaisessa paloriskien arvioinnissa sekä laskennallisesti tehokkaan säteilylämmönsiirron ratkaisijan kehittäminen Fire Dynamics Simulator -ohjelmaan.

Työn ensimmäisessä osassa on kehitetty insinöörikäyttöön soveltuva, Probabilistic Fire Simulator (PFS) -niminen työkalu paloriskien arviointiin. PFS-työkalulla tulipaloa voidaan tutkia Monte Carlo -menetelmällä, jossa simulointeja toistetaan useita kertoja satunnaisilla syöteparametrien arvoilla, jolloin yksittäisen numeroarvon sijaan tuloksena saadaan tulosten jakauma. Käytännön sovelluksissa tarvitaan numeeriseen virtauslaskentaan perustuvia simulointimenetelmiä, koska simuloitavat tilavuudet ovat suuria ja monimutkaisia ja koska niissä pitää pystyä simuloimaan palon leviämistä. Monte Carlo -menetelmän toteutuksessa on tällöin käytettävä tehtävään sopivia erikoismenetelmiä, koska virtauslaskenta on laskennallisesti raskasta ja aikaa vievää. Tässä työssä kehitetyn Kahden mallin Monte Carlo -menetelmän avulla laskentaa voidaan nopeuttaa yhdistämällä kahden eritasoisen mallin tulokset. Nopeasti ratkaistavan mutta epätarkan mallin tuottamia tuloksia parannetaan hitaammin ratkaistavan mutta tarkemman mallin avulla. Menetelmää on testattu erilaisilla palomallien yhdistelmillä aina analyyttisistä kaavoista virtauslaskentaan asti.

Työn toisessa osassa on kehitetty säteilylämmönsiirron numeerinen ratkaisija Fire Dynamics Simulator -ohjelmaan. Ratkaisija laskee säteilyn etenemistä palokaasuja, nokea ja nestepisaroita sisältävässä väliaineessa. Palokaasujen ja noen muodostaman seoksen säteilyominaisuudet lasketaan keskiarvoistamalla RadCal-kapeakaistamallin tulokset aallonpituuden yli. Lämpösäteilyn eteneminen ratkaistaan säteilylämmönsiirron kontrollitilavuusmenetelmällä. Säteilyratkaisijan vaatima laskenta-aika saadaan alle 30 %:iin kokonaislaskenta-ajasta käyttämällä eksplisiittistä ratkaisumenetelmää ja tehokkaita taulukkohakuja sekä luopumalla ratkaisun aikatarkkuudesta. Tarkkuutta voidaan tarvittaessa parantaa jakamalla tarkasteltava aallonpituusalue veden ja hiilidioksidin tärkeimpiä absorptiokaistoja vastaaviin osiin sekä tihentämällä diskretointia avaruuskulman ja ajan suhteen. Työssä on kehitetty uusi laskenta-malli nestepisaroiden ja säteilyn vuorovaikutukselle. Pisaroiden säteilyominaisuudet lasketaan Mie-teorian avulla ja keskiarvoistetaan sekä spektrin että pisarakokojakauman yli. Yksittäisen nestepisaran sirottaman energian vaihe-funktiota approksimoidaan eteenpäin siroavien ja isotrooppisten komponenttien summana. Säteilyratkaisijaa on testattu vertaamalla laskettuja tuloksia analyyttisiin ja kokeellisiin tuloksiin.

ISBN
978-951-38-7099-7 (nid.)
978-951-38-7100-0 (URL: http://www.vtt.fi/publications/index.jsp)

| Avainnimeke ja ISSN | Projektinumero |
|---|---|
| VTT Publications<br>1235-0621 (nid.)<br>1455-0849 (URL: http://www.vtt.fi/publications/index.jsp) | |

| Julkaisuaika | Kieli | Sivuja |
|---|---|---|
| Toukokuu 2008 | Englanti, suom. tiiv. | 103 s. + liitt. 82 s. |

| Avainsanat | Julkaisija |
|---|---|
| fire simulation, Monte Carlo simulation, probabilistic risk assessment, thermal radiation, verification, validation | VTT<br>PL 1000, 02044 VTT<br>Puh. 020 722 4520<br>Faksi 020 722 4374 |

An essential part of fire risk assessment is the analysis of fire hazards and fire propagation. In this work, models and tools for two different aspects of numerical fire simulation have been developed. In the first part of the work, an engineering tool for probabilistic fire risk assessment has been developed. The tool can be used to perform Monte Carlo simulations of fires and is called Probabilistic Fire Simulator (PFS). By the use of the Two-Model Monte Carlo (TMMC) technique, developed in this work, the computational cost of the simulation can be reduced significantly by combining the results of two different models.

In the second part of the work, a numerical solver for thermal radiation has been developed for the Fire Dynamics Simulator code. The solver can be used to compute the transfer of thermal radiation in a mixture of combustion gases, soot and liquid droplets. A new model has been developed for the absorption and scattering by liquid droplets. The radiation solver has been verified by comparing the results against analytical solutions and validated by comparisons against experimental data from pool fires and experiments of radiation attenuation by water sprays at two different length scales.

Julkaisu on saatavana
VTT
PL 1000
02044 VTT
Puh. 020 722 4520
http://www.vtt.fi

Publikationen distribueras av
VTT
PB 1000
02044 VTT
Tel. 020 722 4520
http://www.vtt.fi

This publication is available from
VTT
P.O. Box 1000
FI-02044 VTT, Finland
Phone internat. + 358 20 722 4520
http://www.vtt.fi

ISBN 978-951-38-7099-7 (soft back ed.)
ISSN 1235-0621 (soft back ed.)

ISBN 978-951-38-7100-0 (URL: http://www.vtt.fi/publications/index.jsp)
ISSN 1455-0849 (URL: http://www.vtt.fi/publications/index.jsp)

Hostikka